

Improving radar-based rainfall nowcasting by a nearest neighbour approach: Part I – Storm Characteristics

Bora SHEHU¹, Uwe HABERLANDT¹

¹Institute for Hydrology and Water Resources Management, Leibniz University Hannover, Germany

Correspondence to: Bora Shehu (shehu@iww.uni-hannover.de)

Abstract.

The nowcast of rainfall storms at fine temporal and spatial resolutions is quite challenging due to the unpredictable nature of rainfall at such scales. Typically, rainfall storms are recognized by weather radar, and extrapolated in the future by the Lagrangian persistence. However, storm evolution is much more dynamic and complex than the Lagrangian persistence, leading to short forecast horizons especially for convective events. Thus, the aim of this paper is to investigate the improvement that past similar storms can introduce to the object-oriented radar based nowcast. Here we propose a nearest neighbour approach that measures first the similarity between the “to-be-nowcasted” storm and past observed storms, and later uses the behaviour of the past most similar storms to issue either a single nowcast (by averaging the 4 most similar storm-responses) or an ensemble nowcast (by considering 30 most similar storm-responses). Three questions are tackled here: i) what features should be used to describe storms in order to check for similarity? ii) how to measure similarity between past storms? and iii) is this similarity useful for object-oriented nowcast? For this purpose, individual storms from 110 events in the period 2000-2018 recognized within the Hannover Radar Range (R~115km²), Germany, are used as a basis for investigation. A “leave-one-event-out” cross-validation is employed to test the nearest neighbour approach for the prediction of the area, mean intensity, the x and y velocity components, and the total lifetime of the “to-be-nowcasted” storm for lead times from +5min up to + 3 hours. Prior to the application, two importance analyses methods (Pearson correlation and partial information correlation) are employed to identify the most important predictors. The results indicate that most of storms behave similarly, and the knowledge obtained from such similar past storms helps to capture better the storm dissipation, and improves the nowcast compared to the Lagrangian persistence especially for convective events (storms shorter than 3 hours) and longer lead times (from 1 to 3 hours). The main advantage of the nearest neighbour approach is seen when applied in a probabilistic way (with the 30 closest neighbours as ensembles) rather than in a deterministic way (averaging the response from 4 closest neighbours). The probabilistic approach seems promising, especially for convective storms, and it can be further improved by either increasing the sample size, employing more suitable methods for the predictor identification, or selecting physical predictors.

Keywords:

Rainfall nowcast, Lagrangian persistence, probabilistic nowcast, similar storms, nearest neighbour

31 1. Introduction

32 Urban pluvial floods are caused by short, local and intense rainfall convective storms, that overcome rapidly the
33 drainage capacity of the sewer network and lead to surface inundations. These types of floods are becoming more relevant
34 with time due to the expansion of urban areas worldwide (Jacobson, 2011; United, 2018), and the potential of such storms
35 getting more extreme under the changing global climate (Van Dijk et al., 2014). Because of the high economical, and
36 even human losses associated with these floods, modelling and forecasting becomes crucial for impact-based early
37 warnings (i.e. July 2008 in Dortmund (Grünewald, 2009), August 2008 in Tokyo (A. Kato & Maki, 2009)). However, one
38 of the main challenges in the urban pluvial flood forecasting, remains the accurate estimation of rainfall intensities at very
39 fine scales. Since the urban area responds fast and locally to the rainfall (due to the sealed surfaces and the artificial
40 deviation of watercourse), the Quantitative Precipitation Forecasts (QPFs) fed into the urban models should be provided
41 at very fine temporal (1-5min) and spatial ($100\text{m}^2 - 1\text{km}^2$) scales (Berne et al., 2004). The Numerical Weather Prediction
42 Models (NWP) are typically used in hydrology for weather forecast to several days ahead, nevertheless they are not
43 suitable for urban modelling as they still cannot produce reliable and accurate intensities for spatial scales smaller than
44 10km^2 and temporal time steps shorter than an hour (R. Kato et al., 2017; Surcel et al., 2015). Ground rainfall
45 measurements (rain-gauges) are considered the true observation of rainfall but they are as well not adequate for QPFs
46 because, due to the sparsity of the existing rain-gauge networks, they cannot capture the spatial structure of rainfall.
47 Therefore, the only product useful in providing QPFs for urban pluvial floods remains the weather radar. The weather
48 radar can measure indirectly the rainfall intensities at high spatial ($\sim 1\text{km}^2$) and temporal ($\sim 5\text{min}$) resolutions by capturing
49 the reflected energy from the water droplets in the atmosphere. The rainfall structures and their evolution in time and
50 space can be easily identified by the radar and hence serve as a basis for issuing QPFs at different forecast horizons. One
51 of the main drawbacks of radar-based forecast, is that a rainfall structure has to be first identified in order to be
52 extrapolated in the future. In other words, rainfall cannot be predicted before it has started anywhere in the region, only
53 the movement can be predicted. As already discussed in Bowler et al., (2006) and Jensen et al. (2015), these initialization
54 errors cause the radar forecast to be used only for short forecast horizons (up to 3 hours), and that is why are typically
55 referred to as nowcasts. For longer lead times a blending between NWP and radar based nowcasts should be used instead
56 (Codo & Rico-Ramirez, 2018; Foresti et al., 2016; Jasper-Tönnies et al., 2018). Nonetheless, for short forecast horizons
57 up to 2-3h, the radar nowcast remains the best product for pluvial flood simulations as it outperforms the NWP one
58 (Berenguer et al., 2012; Jensen et al., 2015; Lin et al., 2005; Zahraei et al., 2012).

59 Two approaches can be distinguished on the radar based QPFs depending on how the rainfall structures are
60 identified, tracked and extrapolated into the future: object-oriented nowcasting (herein as object-based to avoid the
61 confusion with the programming term) and field-based nowcasting. The object-based nowcast treats rainfall structures as
62 objects, each object is regarded as a storm and is defined as a set of radar grid cells that moves together as a unit (Dixon
63 & Wiener, 1993). The field-based approach considers the rainfall as an continuous field inside a given domain, and
64 through methods like optical flow, tracks and extrapolates how the intensity is moving from one pixel to the other inside
65 this domain (Ruzanski et al., 2011; Zahraei et al., 2012). Convective storms have been proven to have a unique movement
66 from nearby storms (Moseley et al., 2013), thus are thought to be better nowcasted with object-based approach
67 (Kyznarová & Novák, 2009). On the other hand, the field-based approach with an optical flow solution, tracks and
68 extrapolates rainfall structures inside a region together as a unit with a constant velocity (Lucas & Kanade, 1981) and are
69 considered more suitable for major scale events, i.e. stratiform storms, as they are widespread in the radar image and
70 exhibit more uniform movements (Han et al., 2009). Even though the field-based approach has gained popularity
71 recently (Ayzel et al., 2020; Imhoff et al., 2020) they still have trouble nowcasting convective storms. Thus, the focus in

72 this study is on object-based nowcasts as they are more convenient for convective storms that typically cause urban pluvial
73 floods.

74 **Figure 1** illustrates the three main steps performed in an object-based nowcast: a) first the storm is identified –a
75 group of grid cells with intensity higher than a threshold is recognized in the radar image at time t_0 , b) the storm identified
76 is then tracked for the time $t_0+\Delta t$ (where Δt is the temporal resolution of the radar data) and velocities are assigned from
77 consecutive storm objects, and finally c) the storm as lastly observed at time t (when the nowcast is issued) is extrapolated
78 at a specific lead time (the time in the future when the forecast is needed) t_{+LT} , with the last observed velocity vector. This
79 is a linear extrapolation of the storm structure in the future, considering the spatial structure and the movement of the
80 storm as constant in time - also referred to as Lagrangian Persistence (Germann et al., 2006). Applications of such storm-
81 based nowcast are common in literature like TITAN, HyRaTrac, Konrad etc. (Han et al., 2009; Hand, 1996; Krämer, 2008;
82 Lang, 2001; C. E. Pierce et al., 2004).

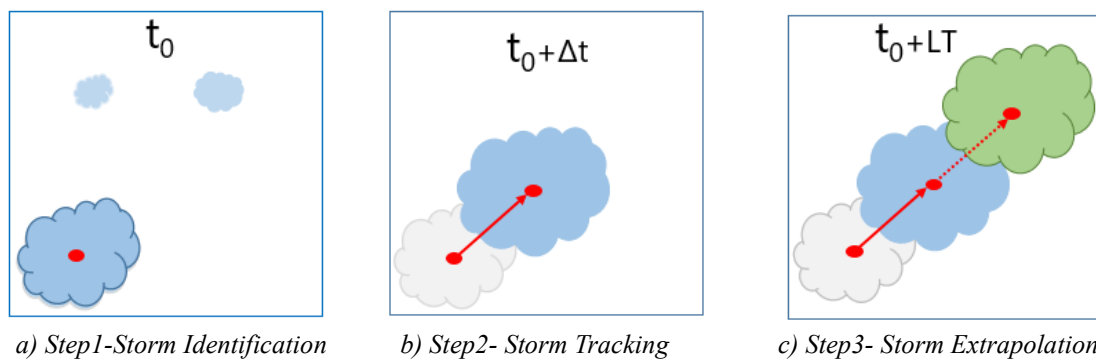


Figure 1 The main steps of an object-based radar nowcast. Blue indicates the current state of the storm at any time t , grey indicates the past states of the storm (at $t_0+\Delta t$), and green indicates the future states of the storm (t_0+LT) (Shehu, 2020)

83 Apart from the initialization errors mentioned before, other error sources in the object-based nowcast can be
84 attributed to storm identification, storm tracking and Lagrangian extrapolation (L. Foresti & Seed, 2015; C. Pierce et al.,
85 2012; Rossi et al., 2015). Many works have been already conducted to investigate the role of different intensity thresholds
86 on the storm identification, or of different storm tracking algorithms on the nowcasting results (Goudenhoofd & Delobbe,
87 2013; Han et al., 2009; Hou & Wang, 2017; Jung & Lee, 2015; Kober & Tafferner, 2009). Very high intensity thresholds
88 may be suitable for convective storms, however can cause false splitting of the storms and which can affect negatively
89 the tracking algorithm. Thus, one has to be careful in adjusting the intensity threshold dynamically over the radar field
90 and type of storm. Storm tracking algorithm can be improved if certain relationships are learned from past observed
91 dataset (like a Fuzzy approach in Jung & Lee (2015) or a tree-based structure in Hou & Wang (2017)), but there is still a
92 limit that the tracking improvement cannot surpass due to the implementation of the Lagrangian persistence (Hou & Wang,
93 2017). These errors due to the Lagrangian persistence are particularly high for convective events at longer lead times (past
94 1 hour) as the majority of convective storms dissipate within 60 minutes (Goudenhoofd & Delobbe, 2013; Wilson et al.,
95 1998). At these lead times, the persistence fails to predict the dissipation of these storm cells, while for shorter lead times
96 it fails to represent the growing/decaying rate and the changing movement of a storm cell (Germann et al., 2006). For
97 stratiform events, since they are more persistent in nature, Lagrangian persistence can give reliable results up to 2 or 3
98 hours lead time (Krämer, 2008). Nevertheless studies have found that for fine spatial (1km^2) and temporal (5min) scales,
99 the Lagrangian Persistence can yield reliable results up to 20-30 min lead time, which is also known in the literature as
100 the predictability limit of rainfall at such scales (Greco & Krajewski, 2000; R. Kato et al., 2017; Ruzanski et al., 2011).
101 In object-based radar nowcast, this predictability limit can be extended up to 1 hour for stratiform events and up to 30-

102 45min for convective events if a better radar product (merged with rain gauge data) is fed into the nowcast model (Shehu
103 & Haberlandt, 2021). Past these lead times, the errors due to the growth/decay and dissipation of the storms dominate.

104 The predictability of convective storms can be extended, if instead of the Lagrangian persistence, one estimates
105 these non-linear processes (growth/decay/dissipation) by utilizing storm life characteristics analysed from past
106 observations (Goudenhoofd & Delobbe, 2013; Zawadzki, 1973). For instance, (Kyznarová & Novák, 2009) used the
107 CellTrack algorithm to derive life cycle characteristics of convective storms and observed that there is a dependency
108 between storm area, maximum intensity, life phase and height of 0°C isotherm level. Similar results were also found by
109 (Moseley et al., 2013) which concluded that convective storms show a clear life cycle with the peak occurring at 1/3 of
110 total storm duration, a strong dependency on the temperature and increasing average intensity with longer durations. In
111 case of extreme convective storms, earlier peaks are more obvious causing a steeper increase to maximum intensity. A
112 later study by (Moseley et al., 2019) found that the longest and most intense storms were expected in the late afternoon
113 hours in Germany. Thus, it is to be expected that an extensive observation of past storm behaviours can be very useful in
114 creating and establishing new nowcasting rules (Wilson et al., 2010) that can outperform the Lagrangian persistence. An
115 implementation of such learning from previous observed storms (with focus only on the object-based nowcast and not the
116 field-based one) is for instance shown by (Hou & Wang, 2017) where a Fuzzy classification scheme was implemented to
117 improve the tracking and matching of storms which resulted in an improved nowcast, and Zahraei et al. (2013) where a
118 Self-Organizing-Maps (SOM) algorithm was used to predict the initialization and dissipation of storms on coarse scales
119 extending the predictability of storms by 20%. These studies suggest that past observed relationships may be useful in
120 extending the predictability limit of the convective storms. Under this context, a nearest neighbour method (k-NN) may
121 be developed at the storm scale and used to first recognize similar storms in the past, and then assign their behaviours to
122 the “to-be-nowcasted” storm. The nearest neighbour method has been used in the field of hydrology mainly for
123 classification, regression or resampling purposes (e.g. Lall & Sharma (1996)) but there are some examples of prediction
124 as well (Galeati, 1990). The assumption of this method is that similar events are described by similar predictors, and if
125 one identifies the predictors successfully, similar events that behave similarly can be identified. For a new event, the
126 respective response is then obtained by averaging the responses of past k – most similar storms. The k-value can be
127 optimized by minimizing a given cost function. Because of the averaging, the response obtained, will be a new one,
128 satisfying thus the condition that nature doesn’t repeat itself, but nevertheless it is confined within the limits of the
129 observed events (therefore is unable to predict extreme behaviours outside of the observed range).

130 Similar approaches are implemented in field-based nowcast (referred to as analogue events), where past similar
131 radar fields are selected based on weather conditions and radar characteristics i.e. in NORA nowcast by (Panziera et al.,
132 2011) mainly for orographic rainfall, or in the multi-scaled analogues nowcast model by (Zou et al., 2020). Panziera et
133 al. 2011 showed that there is a strong dependency between air-mass stability, wind speed and direction and the rainfall
134 patterns observed from the radar data, and that the NORA nowcast can improve the hourly nowcasts of orographic rain
135 up to 1 hour when compared to Eulerian Persistence and up to 4 hours when compared with the COSMO2 NWP.
136 Improvement of predictability through a multi-scaled analogues nowcast was also reported by (Zou et al., 2020), which
137 identified neighbours first by accounting similar meteorological conditions and then the spatial information from radar
138 data. However, both of these studies show the applicability of the method on rainfall types that tend to repeat the rainfall
139 patterns; i.e. the orographic forcing in the case of Panziera et al. (2011) and winter stratiform events in the case of Zou et
140 al. (2020). So far, to the authors knowledge, such application of the k-NN has not been applied for convective events.
141 This application seems reasonable as an extension of the object-based radar nowcast, in order to treat each convective
142 storm independently. It can be used instead of the Lagrangian persistence in step 3 in **Figure 1-c**, for the extrapolation of
143 rainfall storms into the future. Moreover, the benefit of the k-NN application is that one can either give a single or an

144 ensemble nowcast; since k-neighbours can be selected as similar to a storm at hand, a probability based on the similarity
145 rank, can be issued at each of the past storm, providing so an ensemble of responses, which are more preferred compared
146 to the deterministic nowcast due to the high uncertainty associated with rainfall predictions at such fine scales (Germann
147 & Zawadzki, 2004). Thus, it is the aim of this study to investigate the suitability of the k-NN application to substitute the
148 Lagrangian Persistence in the nowcasting of mainly convective events that have the potential to cause urban pluvial floods.

149 We would like to achieve this by first investigating if a K-NN is able to nowcast successfully storm characteristics
150 like Area, Intensity, Movement and Total Lifetime for different life cycles and lead times. Based on the observed
151 dependency of the storm characteristics on the life cycle, it would be interesting to see if the morphological features are
152 enough to describe the evolution of the convective storms. Therefore, the focus is here only of the features recognized by
153 the radar data, and further works will include as well the use of meteorological factors. To reach our aim, the suitability
154 of the k-NN approach is studied as an extension of the existing object-based nowcast algorithm HyRaTrac developed
155 from Krämer (2008). Before such an application, questions that arise are I) what features are more important when
156 describing a storm, II) how to evaluate similarity between storms and III) how to use their information for nowcasting the
157 storm at hand. The paper is organized as follows: first in Section 2 the study area is described, following with the structure
158 of the k-NN method in Section 3.1 where: the generation of the storm database is discussed in Section 3.1.1, the predictors
159 selected and target variables are given in in Section 3.1.2, the methods used for predictor identification in Section 3.1.3,
160 and different application of the k-NN in Section 3.1.4. The optimization and the performance criteria are shown in Section
161 3.2 followed by the results in Section 4 separated into predictors influence (Section 4.1), deterministic k-NN (Section
162 4.2), probabilistic k-NN performance (Section 4.3), and the nowcasting of unmatched storms (Section 4.4). Finally, the
163 study is closed with conclusions and outlook in Section 5.

164 2. Study Area and Data

165 The study area is located in northern Germany, and lies within the Hannover Radar Range as illustrated in **Figure**
166 **2**. The radar station is situated at the Hannover Airport, and it covers an area with a radius of 115 km. The Hannover radar
167 data are C-band data (single-pol) provided by German Weather Service (DWD), and measure the reflectivity at an azimuth
168 angle of 1° and at 5 min scans (Winterrath et al., 2012). The reflectivity is converted to intensity according to Marshall-
169 Palmer relationship with the coefficients $a=256$ and $b=1.42$ (Bartels et al., 2004). The radar data are corrected from the
170 static clutters and erroneous beams and then converted to Cartesian Coordinate system (1 km² and 5 min) as described in

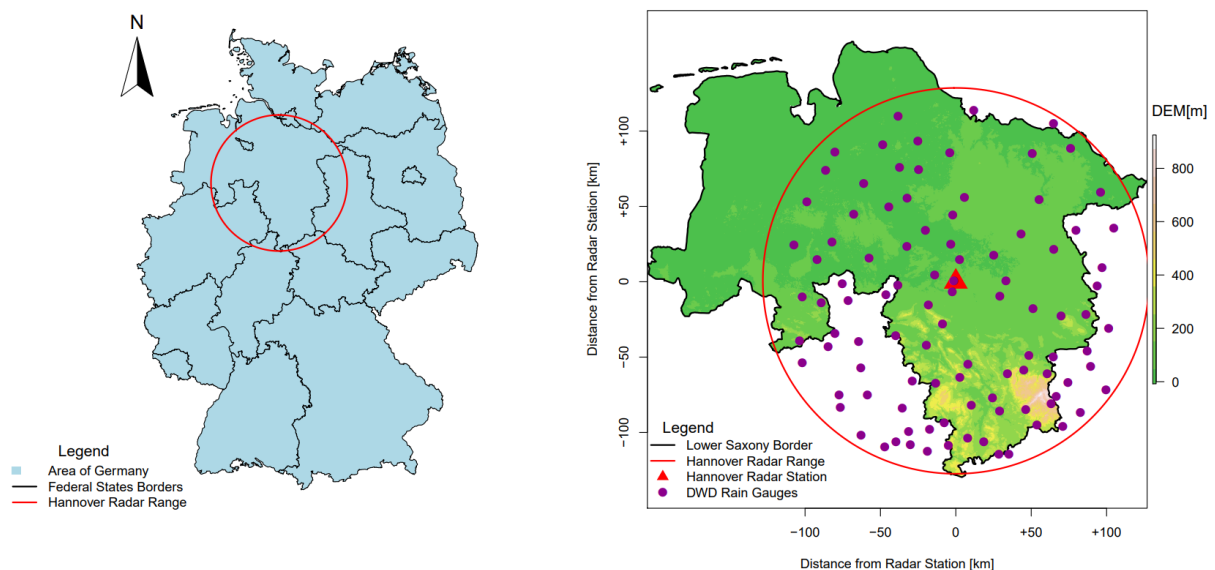


Figure 2 The location of the study area (left) within Germany and (right) with the corresponding elevation and boundaries, and as well with the available recording rain gauges (purple) and radar (red) station. The DEM is short for Digital Elevation Model (adapted from Shehu and Haberlandt, 2021).

171 (Berndt et al., 2014), while the rain-gauges measure the rainfall intensities at 1 min temporal resolution but are aggregated
 172 to 5min time steps. Additionally, following the results from Shehu & Haberlandt (2021), a conditional merging between
 173 the radar data and 100 rain-gauge recording (see **Figure 2** -right) with the radar range at 5 min time steps is performed.
 174 The conditional merging aims to improve the kriging interpolation of the gauge recordings by adding the spatial variability
 175 and maintaining the storm structures as recognized by the radar data. In case a radar image is missing, the kriging
 176 interpolation of the gauge recordings is taken instead.

177 The period from 2000 to 2018 is used as a basis for this investigation, from which 110 events with different
 178 characteristics were extracted (see Shehu & Haberlandt (2021) or Shehu (2020)). These events were selected for urban
 179 flood purposes, and contain mainly convective events and few stratiform ones. Here, rainfall events are referred to a time
 180 period when rainfall has been observed inside the radar range and at least at one rain gauge has registered an extreme
 181 rainfall volume (return period higher than 5 years) for durations varying from 5 min to 1 day. The start and the end of the
 182 rainfall event is determined when areal mean radar intensity is higher/lower than 0.05mm for more than 4 hours. Within
 183 a rainfall event many rainfall storms, at different times and locations, can be recognized. **Figure 3**-a shows a simple
 184 illustration to distinguish between the rainfall event and rainfall storm concepts employed in this study.

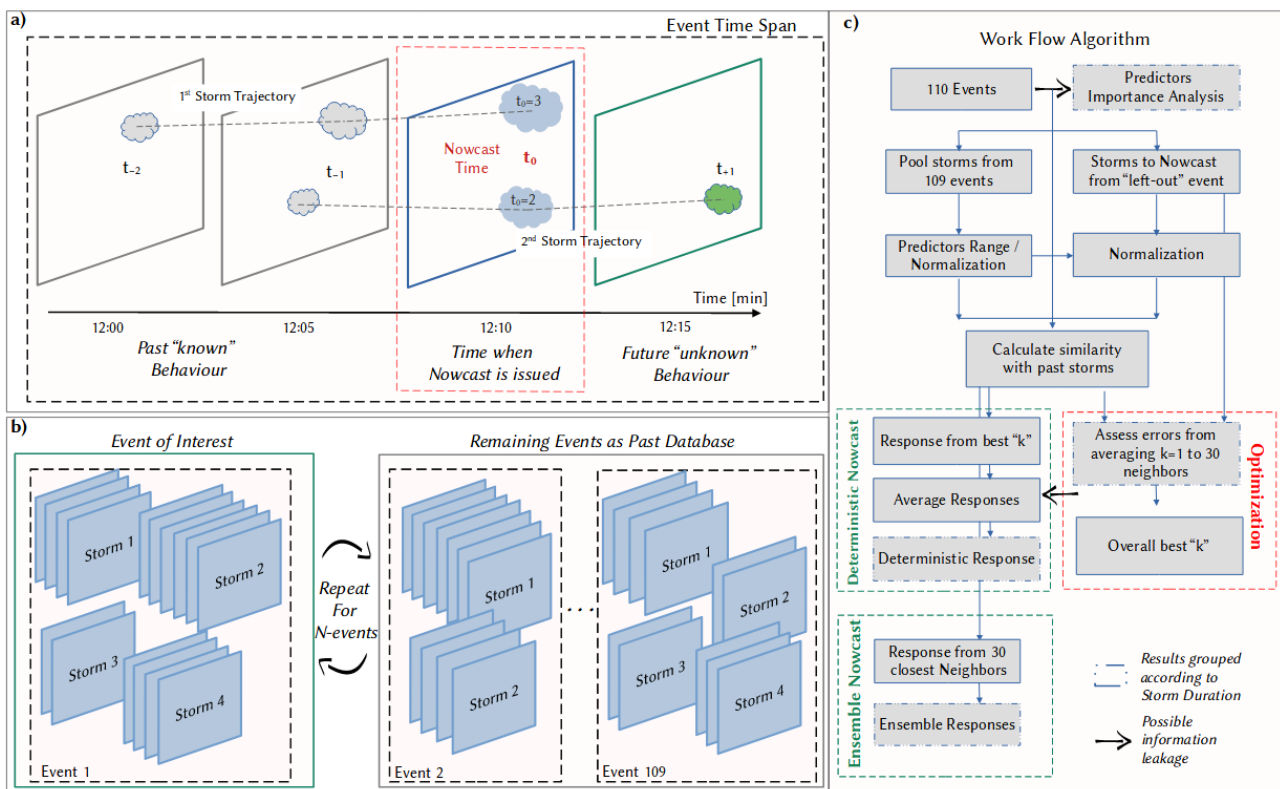


Figure 3 Illustration of concepts and workflows in this study a) an event contains many rainfall storms inside the radar range which are tracked and nowcasted: the dashed grey lines indicate the movements of storms in space-time within the radar event and the event time span. b) The "leave-one-out-event cross-validation" – the storms of the event of interest are removed from the past database, and the nowcast of these storms is issued based on the past database. This process is repeated 110 times (once for each event). c) the workflow implemented here for the optimization and application of the k -NN approach.

185 3. Methods

186 3.1 Developing the k-NN model

187 3.1.1 Generating the storm database

188 Each of the selected events contains many storms, whose identification and tracking was performed on the basis
189 of the HyRaTrac algorithm in the hindcast mode (Krämer, 2008; Schellart et al., 2014). A storm is initialized if a group
190 of spatially connected radar grid cells (> 64) has a reflectivity higher than $Z=20\text{dBz}$, while storms are recognized as
191 convective – if a group bigger than 16 radar grid cells has an intensity higher than 25 dBz, and as stratiform – if a group
192 bigger than 128 radar grid cells has an intensity higher than 20 dBz. Typically, higher values (40dBz) are used to identify
193 the core of convective storms (as in E-Titan), but to avoid false splitting of convective storms and to test the methodology
194 on all types of storms, these identification thresholds were kept low (following as well the studies from Moseley et al.
195 2013). Once storms at different time steps are recognized, they are matched as evolution of a single storm, if the centre
196 of intensity of storm at $t=0$ falls within the boundary box of the storm at $t-5$ min. The tracking of individual storms in
197 consecutive images is done by the cross-correlation optimization between the last 2 images ($t=0$ and $t-5$ min), and local
198 displacement vectors for each storm are calculated. In case a storm is just recognized (the storm does not yet have previous
199 history), then global displacement vectors based on cross-correlation of the entire radar image are assigned to them. It is
200 usually the case, that two storms merge together at a certain time, or a single storm splits between several daughter storms.
201 The splitting and merging of the storms is considered here if two criteria are met: a) the minimum distance between the
202 storms that have splatted or merged is smaller than the perimeter of the merged or that-is-splitting storm, and b) the
203 position of the centre of intensity of former/latter storms is within the boundaries of the latter/former storm.

204 Thus, a dataset with several types of storms is built and saved. The storms are saved with an ID based on the
205 starting time and location, and for each time step of the storm evolution the spatial information is saved and various
206 features are calculated. Here the features computed from the spatial information of the rainfall inside the storm boundaries
207 at a given time step (in 5min) of the storms' life, is referred to as the “state” of the storm. A storm that has been observed
208 for 15 minutes, consists of three “states” each occurring at a 5 min time step. For each of the storm states an ellipsoid is
209 fitted to the intensities in order to calculate the major and minor axis and the orientation angle of the major axis. This
210 storm database is the basis for developing the k-NN method and for investigating the similarity between storms. Some
211 characteristics of the identified storms like duration (or also total lifetime of the storm), mean area, maximum intensity,
212 number of splits/merges, local velocity components, and ellipsoidal features, are shown in the **Figure 4**. These storms
213 characteristics were obtained by an hindcast analysis run of all 110 events with the HyRaTrac algorithm which resulted in
214 around 5200 storms. The local velocities in x and y direction are obtained by a cross-correlation optimization within the
215 storm boundary. The duration of the storm is then the lifetime of the radar pixels group as dictated by the threshold used
216 to recognize them and the tracking algorithm that decides if the same storm is observed at continuous time steps. For more
217 information about the tracking and identification algorithm, reader is directed to Krämer (2008).

218 As seen from the number of storms for each duration in **Figure 4**, the unmatched storm cells make the majority
219 of the storms recognized. These are storms that last just 5 min (one-time step) as the algorithm fails to track them at
220 consecutive time steps. These “storms” can either be dynamic clutter from the radar measurement, as they are
221 characterized by small area, circular shapes (small ratio of minor and major axis) and by very high velocities, or artefacts
222 created by low intensity thresholds used for the storm identification, or finally produced by the unrepresentativeness of
223 the volume captured by the radar station. Another thing to keep in mind, is that merged radar are fed to the algorithm for
224 storm recognition, and this affect the storm structures particularly when the radar data is missing. In such case, the ordinary
225 kriging interpolation of rain gauges is given as input, which is well known to smoothen the spatial distribution of rainfall

226 and hence resulting in a short storm characterized by a very large area. Since the “not” matched storms can either be
 227 dynamic clutter or artefacts, they are left outside of the k-NN application. Nonetheless, they are treated shortly in section
 228 4.5.

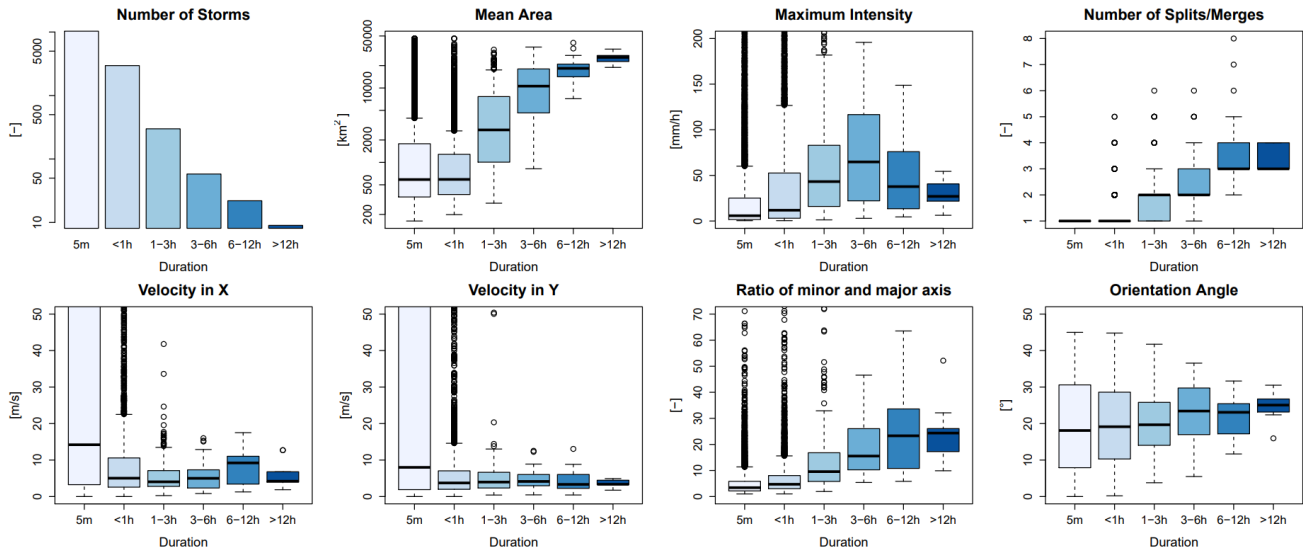


Figure 4 Different properties of the storms recognized from 110 events separated into 6 groups according to their duration (shown in different shades of blue).

229 Apart from the unmatched storms, the majority of the remaining storms are of convective nature: storms with
 230 short duration (shorter than 6 hours), high intensity and low areal coverage. Here two types of convective storms are
 231 distinguished: local convective with very low coverage (on average lower than 1000 km²) and low intensity (on average
 232 ~ 5 mm/h), and mesoscale convective which are responsible for floods (with intensity up to 100 mm/h or more) and have
 233 a larger coverage (on average lower than 5000 km²). The stratiform storms characterized by large area, long duration and
 234 low intensities, as well as meso- γ scale convective events with duration up to 6 hours, are not very well represented by
 235 the dataset as only a few of them are present in the selected events (respectively circa 20 and 50 storms). Therefore, it is
 236 to be expected for the k-NN approach not to yield very good results for such storms due to the low representativeness.
 237 From the characteristics of the storms illustrated in **Figure 4**, it can be seen that for stratiform storms that live longer than
 238 twelve hours the variance of the characteristics is quite low (when compared to the rest of the storms) which can either
 239 be attributed to the persistence of such storms or to the low representativeness in the database. Even though the data size
 240 for stratiform is quite small, the k-NN may still deliver good results as characteristics of such storms are more similar.
 241 Nevertheless, the stratiform storms are typically nowcasted well by the Lagrangian persistence (specially by a field-
 242 oriented approach) as they are wide-spread and persistent. Hence the value of the k-NN is primarily seen for convective
 243 storms and not for stratiform ones.

244 3.1.2 Selecting features for similarity and target variables

245 At first storms are treated like objects that manifest certain features (predictors) like area, intensity, lifetime etc.,
 246 at each state of the storms' life until the storm dissipates (and the predictors are all set to zero). The features of the objects
 247 are categorized into present and past features, as illustrated in **Figure 5** (shown respectively in blue and grey). The present
 248 features describe the current state of the storm at the time of nowcast (denoted with t_0 in **Figure 5**), and are calculated
 249 from one state of the storm. To compute certain features, an ellipsoid is fitted to each state of the storm. The past features,
 250 on the other hand, describe the predictors of the past storm states (denoted with t_{-1} , t_{-2} in **Figure 5**) and their change over
 251 the past life of the storm. For example, the average area from time t_{-2} to t_{-1} is a past feature. A pre-analysis of important
 252 predictors showed that the average features over the last 30 minutes are more suitable as past predictors than the averages

253 over last 15 or 60 min or than the calculation of past changing rates. Therefore, averages over past 30 minutes are
 254 computed here:

$$255 \quad P_{30} = \sum_{i=t_0}^{t-30min} P_i / 7, \quad (1)$$

256 where P_i is the predictors value at time i , and P_{30} the average value of the predictor over last 30min. In case of missing
 257 values, the remaining time steps are used for averaging. The selected features (both present and past) that are used here
 258 to describe storms as objects, and hence tested as predictors, are shown in **Table 1**. The present features help to recognize
 259 storms that are similar at the given state when the nowcast is issued (blue storm in **Figure 5**) and the past ones give
 260 additional information about the past evolution of the storm (average of grey storms in **Figure 5**). The aim of these features
 261 is to recognize the states of previously observed storms that are most similar to the current one (shown in blue in **Figure**
 262 **5**) of the “to-be-nowcasted” storm. Once the most similar past storm states are recognized, their respective future states
 263 at different lead times can be assigned as the future behaviour (shown in green in **Figure 5**) of the current state of the “to-
 264 be-nowcasted” storms. Since the storms are regarded as objects with specific features, future behaviours at different lead
 265 times are determined by four target variables: area (A_{+LT}), mean intensity (I_{+LT}) and velocity in X (V_{X+LT}) and Y (V_{Y+LT})
 266 direction. Additionally, the total lifetime of the storm is considered as a fifth target (L_{tot}). Theoretically, the total lifetime
 267 is predicted indirectly when any of the first four targets is set to zero, however here it is considered as an independent
 268 variable in order to investigate if similar storms have similar lifetime durations.

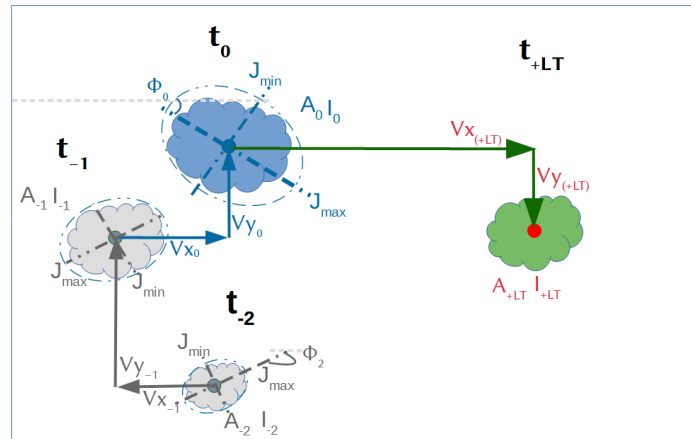


Figure 5 The features describing the past (grey) and present (blue) states of the storm used as predictors to nowcast the future states of the storm (green) at a specific lead time (T_{+LT}) that are described by 4 target variables (in red). The nowcast is issued at time t_0 . A full description of these predictors and target variables is given in **Table 1**.

269 For each state of each observed storm in the database, the past and present features of that state with its' respective
 270 future states of the five target variables from +5min to +180min (every 5 min) lead times are saved together and form the
 271 predictor-target database that is used for the development of the k-NN nowcast model. A summary of the predictors and
 272 target variables calculated per state is given in **Table 1**. Before optimizing and validating the k-NN method (advise **Figure**
 273 3- c), an importance analysis is performed for each of the target variables in order to recognize the most important
 274 predictors. As the predictors have different ranges, prior to the importance analysis and the k-NN application, they are
 275 normalized according to their median and range between the 0.05 and 0.95 quantiles:

$$276 \quad normP_i = \frac{P_i - Q_{P_i}^{0.5}}{Q_{P_i}^{0.95} - Q_{P_i}^{0.05}}, \quad (2)$$

277 where P is the actual value, $normP$ the normalized value, and $Q_{P_i}^{0.5}$, $Q_{P_i}^{0.95}$, $Q_{P_i}^{0.05}$ the quantiles 0.5, 0.05 and 0.95 of the i^{th}
 278 predictors' vector. The reason why these quantiles were used for the normalization instead of the typical mean and
 279 maximum to minimum range, is that some outliers are present in the data. For instance, very high and unrealistic velocities

280 are present in some convective storms where the tracking algorithm fails to capture adequate velocities (Han et al., 2009).
 281 Thus, to avoid the influence of these outliers, the given range is employed.

282 3.1.3 Selection of most relevant predictors

283 The application of the k-NN method can be relevant if there is a clear connection between the target variable and
 284 the features describing this target variable. For instance, in the case of Galeati (1990), a physical background backed up
 285 the connection between target variable (discharge) and the features (daily rainfall volume and mean temperature). In the
 286 case of the storms at such fine temporal and spatial scales, due to the erratic nature of the rainfall itself, there are no
 287 physical related information that can be extracted from radar data. Different features of the storm itself can be investigated
 288 for their importance to the target variable. Nevertheless, the identification of such features (referred here as predictors) is
 289 difficult because it is bounded to the set of the available data and the relationships considered. Commonly a strong Pearson
 290 correlation between the predictors selected and the target variable is used as an indicator of a strong linear relationship
 291 between them. Here, the Pearson correlation absolute values are used directly as predictors weights in the k-NN
 292 application. However, the relationship between predictors and target variables may still be of non-linear nature, thus
 293 another predictor importance analysis should be advised when selecting the predictors. Sharma & Mehrotra (2014)
 294 proposed a new methodology, designed specifically for the k-NN approach, where no prior assumption about the system
 295 type is required. The method is based on a metric called the Partial Information Correlation and is computed from the
 296 Partial Information as:

$$297 \quad PIC = \sqrt{(1 - \exp(-2PI))} \text{ with } PI = \int f_{X,P|Z}(x, p|z) \log \left[\frac{f_{X|Z,P|Z}(x, p|z)}{f_{X|Z}(x|z) f_{P|Z}(p|z)} \right] dx dp dz \quad , \quad (3)$$

298 where PIC is the Partial Information Correlation, PI is the Partial Information which represents the partial dependence of
 299 X on P conditioned to the presence of a predictor Z . The Partial Information itself is a modification of the Mutual
 300 Information in order to measure partial statistical dependency between the predictors (P) and the target variable (X), by
 301 adding predictors one at a time (Z) (step-wise procedure). The evaluation of PIC needs a pre-existing identified predictor
 302 from which the computation can start. If the pre-defined predictor is correctly selected, then through the Equation (3), the
 303 method is able to recognize and leave out the new predictors which are not related to the response and which don't bring
 304 additional value to the existing relationship between the current predictors and target variable. Relative weights for the k-
 305 NN regression application can be derived for each predictor, as a relationship between the PIC metric and the associated
 306 partial correlation:

$$307 \quad \alpha_j = PIC_{X,Z_j|Z(-j)} \frac{S_{X|Z(-j)}}{S_{Z_j|Z(-j)}}, \quad (4)$$

308 where X is the target response, Z_j is the added predictor from the step-wise procedure, $Z(-j)$ previous predictor vector
 309 excluding the predictor Z_j , $S_{X|Z(-j)}$ the scaled conditional standard deviations between target (x) and predictor vector $Z(-j)$,
 310 $S_{Z_j|Z(-j)}$ the scaled conditional standard deviations between the additional predictor (Z_j) and the first predictor vector $Z(-j)$,
 311 and the α_j denotes the predictors weight. The R package NPRED was used for the investigation of the PIC derived
 312 importance weights (Sharma et al., 2016).

313 Here in this study, these two importance analyses are used to determine the most important predictors and their
 314 respective weights in the k-NN similarity calculation. For each target variable the most important predictor identified from
 315 Pearson Correlation, is given to the PIC metric as the first predictor. The analysis is complex due to the presence of several
 316 predictors, 38 states of future behaviour for each target variable (for each 5min between +5min to +180 min lead times),
 317 and different nowcast times; the weights were calculated first for three lead times +15min, +60min and +180 min, and for
 318 three storm groups separated according to their duration <60min, 60min-180min, and > 3 hours. Here the average weights

319 over these groups and lead times are calculated and used as a reference for each importance analysis. The k-NN errors
 320 with these average weights are compared in Section 4.1.

Table 1 List of all the past and present features of the storms that are investigated for their importance as predictors, and the respective target variables calculated for different lead times.

	Features	Symbol
Present Features	number of storm cells within the storm region	Cells [-]
	current storm lifetime at time of nowcast	L_{now} [min]
	area of the storm	A [km ²]
	mean spatial intensity	I_{ave} [mm/h]
	maximum spatial intensity	I_{max} [mm/h]
	standard deviation of the spatial intensities	I_{sd1} [-]
	standard deviation of intensities groups inside the storm	I_{sd2} [-]
	global velocity of the entire radar image	V_g [m/s]
	x and y component of the local velocity of the storm region	V_x, V_y [m/s]
	major and minor axis of the ellipsoid and their ratio	$J_{\text{max}}, J_{\text{min}}$ [km], J_r [-]
orientation angle of the major axis of the ellipsoid	Φ [°]	
Past Features	average area over the last 30 min of storm existence	A_{30} [km ²]
	average mean intensity over the last 30 min of storm existence	$I_{\text{ave}30}$ [mm/h]
	average maximum intensity over the last 30 min of storm existence	$I_{\text{max}30}$ [mm/h]
	average standard deviation of intensity over the last 30 min of storm existence	$I_{\text{sd}130}$ [-]
	average standard deviation of intensity groups over the last 30 min of storm existence	$I_{\text{sd}230}$ [-]
	average global velocity over the last 30 min of storm existence	V_{g30} [m/s]
	average x and y component of the local velocity over the last 30 min of storm existence	V_{x30}, V_{y30} [m/s]
	average value of the major and minor axis of the ellipsoid and their ratio over the last 30 min of storm existence	$J_{\text{max}30}, J_{\text{min}30}$ [km] J_{r30} [-]
	average major axis orientation of the ellipsoid over the last 30 min of storm existence	Φ_{30} [°]
Target Variables	Total lifetime of the storm	L_{tot} [min]
	Estimated Area and Intensity at LT from +5min to +180min	$A_{+\text{LT}}$ [km ²], $I_{\text{ave}+\text{LT}}$ [mm/h],
	Estimated Velocity X and Y at LT from +5min to +180min	$V_{x+\text{LT}}, V_{y+\text{LT}}$ [m/s]

321 3.1.4 Developing the k-NN structure

322 The structure of the proposed k-NN approach at the storm scale is illustrated at **Figure 6** - left) the current “to-
 323 be-nowcasted” storm is shown, while at - right) the past observed storms. First in Step 1, the Euclidean distance between
 324 the most important predictors (either present or past predictors), of past storm states and the current one is calculated to
 325 identify the most-similar states of the past storms (distance between the blue shapes at left and right side of **Figure 6**):

$$326 E_d = \sqrt{\sum_{i=1}^N w_i \cdot (X_i - Y_i)^2}, \quad (5)$$

327 where w is the weight of the respective i^{th} predictor as dictated by the importance analysis (results are shown in **Table 3**),
 328 X the predictor of the “to-be-nowcasted” storm, Y the predictor of a past observed storm, N the total number of predictors
 329 used and E_d the Euclidian distance between the “to-be-nowcasted” and a past observed storm. The assumption made here
 330 is that the smaller the distance, the higher the similarity of future behaviour between the selected storms and the “to-be-
 331 nowcasted” storm. Therefore, in **Step 2** these distances are ranked in an ascending order and 30 past storm states with the

332 smallest distance are selected (**Step 3**). Once the similar past storm states have been recognized (the blue-shape in **Figure**
 333 **6** - right), the future states of these storms (the green-shapes in **Figure 6** - right, each for a specific lead time from the
 334 occurrence of the selected similar blue-state), are treated as future states (the green-shape in **Figure 6** - left) of the “to-
 335 be-nowcasted” storm. In **Step 4**, either a single (deterministic) or an ensemble (probabilistic) nowcast is issued. If a single
 336 nowcast is selected, then the green-instances of the k-neighbours are averaged with weights for each lead time:

$$337 \quad R_{new} = \sum_{i=1}^k Pr_i \cdot R_i, \quad (6)$$

338 where k is the number of neighbours obtained from optimization, R_i and Pr_i (from Equation 7) are respectively the
 339 response and weight of the i^{th} neighbour and the R_{new} the response of the “to-be-nowcasted” storm as averaged from k
 340 neighbours. The response R refers to each of the 5 target variables: Area, Intensity, Velocity in X and Y direction, and
 341 Total Lifetime. Contrary, if a probabilistic nowcast is selected, 30- members ensembles are selected from the closest 30
 342 storms where each member is assigned a probability according to the rank of the respective neighbour storm:

$$343 \quad Pr_i = \frac{(1/Rank_i)}{\sum_{i=1}^k (1/Rank_i)}, \quad (7)$$

344 where k is the selected number of neighbours and $Rank$ and Pr are respectively the rank and the probability weights of
 345 the i^{th} neighbour/ensemble member. An ensemble member is then selected randomly based on the given probability
 346 weights. These probability weights calculated here are as well used for computation of the single nowcast in Equation (6).

347 Since the performance of the single k-NN nowcast is highly dependent on the number of k – neighbours used for
 348 the averaging, a prior optimization should be done in order to select the right k -neighbours that yield the best performance
 349 (as illustrated in **Figure 3-c**). The application of the k-NN can either be done per each target variable independently, or
 350 for all target variables grouped together. In the first approach, the dependency of the target variables between one another
 351 is not assured, they are predicted independently from one another. This is referred here as the target-based k-NN and is
 352 denoted in the results as VS1. The main advantage of this application is that, since the relationship between the target

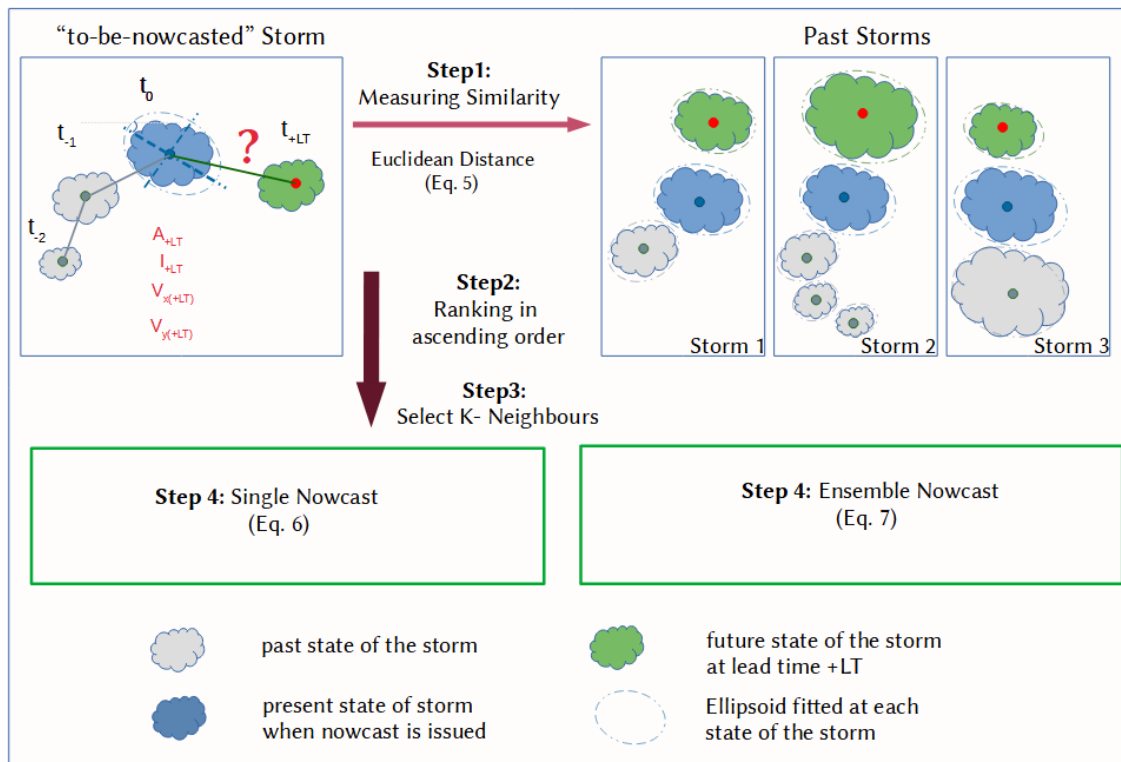


Figure 6 The main steps involved in the k-NN based nowcast with the estimation of similar storms (Step 1 to 3) and assigning the future responses of past storm as the new response of the “to-be-nowcasted” storm either in a deterministic nowcast (Step4-left) or in a probabilistic nowcast (Step4-right).

353 variables are not kept, new storms can be generated. Theoretically, the predicted variables should have a lower error since
 354 the application is done separately per each variable, nevertheless this approach doesn't say much if similar storms behave
 355 similarly. Therefore, it is used here as a benchmark for best possible optimization that can be reached by the k-NN with
 356 the current selected predictor set. In the second approach, the relationships between target variables as exhibited by
 357 previous storms are kept. The storm structure and the relationship between features are maintained as observed and thus
 358 the question if similar storms behave similarly can be answered. This is referred here as the storm-based k-NN and is
 359 denoted in the results as VS2. In this study the two approaches are used (respectively called VS1 and VS2) to understand
 360 the potential and the actual improvement that the k-NN can bring to the storm nowcast.

361 **3.2 Application of the k-NN and performance assessment**

362 **3.2.1 Optimizing the deterministic k-NN nowcast**

363 The optimization of the k-NN is done based on the 5189 storms extracted from 110 events on a “leave-one-out”
 364 cross-validation. Since the “not” matched storms can either be dynamic clutter or artefacts of the tracking algorithm, they
 365 are left outside of the k-NN optimization and validation. The assumption is here that an improvement of the radar data or
 366 tracking algorithm would eliminate the “not” matched storms, hence the focus is only on the improvement that the k-NN
 367 can introduce to the matched storms. “Leave-one-event-out” cross-validation means here that the storms of each event
 368 have to be nowcasted by considering as a past database the storms from the remaining 109 events (a detailed visualization
 369 is given in Figure 3-b). The objective function is the minimization of the mean absolute error (Equation 8) and of the
 370 absolute mean error (Equation 9) between predicted and observed target variables at lead times from +5min to +180 min:

$$371 \quad MAE_{target} = \sum_{i=1}^N (|Pred_{i,+LT} - Obs_{i,+LT}|) / N, \quad (8)$$

$$372 \quad ME_{target} = |\sum_{i=1}^N (Pred_{i,+LT} - Obs_{i,+LT}) / N|, \quad (9)$$

373 where the *Pred* is the predicted response, *Obs* the observed response for the i^{th} storm, *+LT* the lead time and *N* the number
 374 of storms considered inside an event. The results of the storms' nowcast are also dependent on the nowcast time in respect
 375 to the storms' life (time step of the storm existence when the nowcast is issued – refer to Figure 3-a). If the nowcast time
 376 is 5min, only the present predictors are used for the calculation of storm similarity, and as higher the nowcast time, as
 377 more predictors are available for the similarity calculation. It is expected for the nowcast to perform worse at the first
 378 5min of the storm existence, as the velocities are not assigned properly to the storm region and the past predictors are not
 379 yet calculated. Therefore, the optimization is done separately for three different groups of nowcast times, in order to
 380 achieve a proper application of the k-NN model: Group 1 – Nowcast issued at 1st timestep of storm recognition, Group 2
 381 – Nowcast issued between 30min to 1 hour of storm evolution, and Group 3 – Nowcast issued between 2 and 3 hours of
 382 storm evolution. The k-number with the lowest absolute error averaged over all the events for most of the lead times (as
 383 median of MAE from Equation (8) and ME from Equation (9) over all events) is selected as a representative for the
 384 deterministic nowcast.

385 **3.2.2 Validating the k-NN deterministic and probabilistic nowcast**

386 Once the important predictors are identified and the k-NN has been optimized, the performance of both
 387 deterministic and probabilistic k-NN is assessed also in a “leave-one-event-out” cross-validation mode. Two performance
 388 criteria are used to assess the performance:

389 i) absolute error per lead time and target variable computed for each event and a specific selected nowcast time

$$390 \quad MAE_{target} = \sum_{i=1}^N (|Pred_{i,+LT} - Obs_{i,+LT}|) / N, \quad (10)$$

391 where the *Pred* is the predicted response, *Obs* the observed response for the i^{th} storm, *+LT* the lead time and *N* the number
 392 of storms considered inside an event.

393 ii) the improvement (%) per each lead time and target variable that the k-NN approach introduces to the nowcast
 394 (for a specific selected nowcast time) when compared to the Lagrangian persistence in object-based approach;

$$395 \quad Error_{impr} [\%] = 100 \cdot \frac{(|Error_{ref}| - |Error_{new}|)}{|Error_{ref}|}, \quad (11)$$

396 where the $Error_{new}$ is the event error manifested by the k-NN, the $Error_{ref}$ the event error manifested by the Lagrangian
 397 persistence and the $Error_{impr}$ the improvement in reducing the error per each lead time. For improvements higher than
 398 100% or lower than -100%, the values are reassigned to the limits respectively 100% and -100%. Here the Lagrangian
 399 persistence refers to as persistence of the storm characteristics (Area, Intensity, Velocity in X and Y Direction) as last
 400 observed and constant for all lead times.

401 For the probabilistic approach, the Continuous Rank Probability Score (CRPS) as shown in Equation (12) is computed.

$$402 \quad CRPS(F, y) = \int_{-\infty}^{\infty} (F(x) - 1\{y \leq x\})^2 dx = E_F |Y - y| - \frac{1}{2} E_F |Y - Y'| \quad (12)$$

403 where F is a probabilistic forecast, y the observed value, Y and Y' independent random variables with CDF of F and finite
 404 first moment E (Gneiting & Katzfuss, 2014). The CRPS is a generalization of the mean absolute error, thus if a single
 405 nowcast is given, it is reduced to the mean absolute error (Equation 10). This enables a direct comparison between the
 406 probabilistic and deterministic nowcast and to investigate the advantages of the probabilistic one. As in Equation (8), the
 407 values obtained in Equation (10), (11) and (12) are averaged per each of the 110 events.

408 As stated earlier the results depend on the nowcast time and also storm duration (in regard to available storms).
 409 Therefore, the performance criteria for both k-NN nowcasts were computed separately for different storm durations and
 410 nowcast times as illustrated in **Table 2**. It is important to mention as well, that since one event may contain many storms
 411 of similar nature, when leaving one event out for the cross-validation, the number of available storms is actually lower
 412 than the numbers given in **Table 2**. This is particularly affecting the performance of the storms longer than 6 hours, as the
 413 “leave-one-event-out” cross-validation leaves fewer available storms for the similarity computation. Lastly, it is important
 414 to notice, that the performance criteria can be calculated even for nowcast times longer than the storm lifetime, if the
 415 nowcast fails to capture the dissipation of the storms. In this case, Area, Intensity, Velocity in X and Y Direction are
 416 compared against zero, while the Total Lifetime against the total observed lifetime of the storms.

Table 2 The selected storm durations and nowcast times for the performance calculation of the deterministic and probabilistic nowcast and the respective number of storms for each case.

Storm living less than 30 min		Storms living within 0.5 - 3 hours		Storms living longer than 3 hours	
Nowcast Time	No. Storms	Nowcast Time	No. Storms	Nowcast Time	No. Storms
5 min	4106	5 min	994	5min	89
15 min	2265	1h	370	2h	89
30 min	271	3h	6	6h	33

417 **4. Results:**

418 **4.1 Predictors Importance Analysis**

419 **Table 3** illustrates the results of the two important analysis methods (Pearson correlation and partial information
 420 correlations - PIC) for each of the target variable and their average over the 5 variables. The stronger the shade of the
 421 green colour, the more important is the predictor for the target variable. The weights given here are averaged from the
 422 weights calculated at three different lead times and storm durations (see **Appendix 11.1** and **11.2** for more detailed
 423 information about the calculated weights). First the Pearson Correlation weights are advised for the identification of the
 424 most important predictors. From the results it is clear that the autocorrelation has a higher influence, as the target variables
 425 are mostly correlated with their respective past and present values. This influence logically is higher for the shorter lead
 426 times and smaller for the longer lead times. For longer lead times the importance of other predictors, that are not related
 427 directly with the target variable, increases. Similar patterns can be observed among the Area, Intensity and Total Lifetime
 428 target variables, indicating that these three variables may be dependent on each other, and on similar predictors like:
 429 current lifetime, area, standard deviation of intensity, the major and minor ellipsoidal axis and the global velocity. This
 430 conclusion agrees well with the life cycle characteristics of convective storms reported in the literature review. On the
 431 other hand, are the velocity components, which seem to be highly dependent on the autocorrelation and slightly correlated
 432 to area and ellipsoidal axes. It has to be mentioned that apart for the standard deviation intensities also the mean, median,
 433 and maximum spatial intensities were investigated. Nevertheless, it was found that the I_{sd1} and I_{sd2} had the higher
 434 correlation weights, and since there is a high collinearity between these intensity predictors, they were left out of the
 435 predictor's importance analysis.

Table 3 Strength of relationship between the selected predictors and the target variables averaged for three lead times and storm duration groups (original weights can be seen in the Appendix 11.1 and 11.2) based on two predictors identification methods: upper –correlation, and lower –PIC weights. The green shade indicates the strength of the relationship: with 0 for no relationship at all, and 1 for highest dependency.

Method	Target	Present Predictors												Past Predictors - averaged from last 30 min									
		Cells	L_{now}	A	I_{sd1}	I_{sd2}	V_g	V_x	V_y	J_{max}	J_{min}	J_r	Φ	A_{30}	$I_{sd1_{30}}$	$I_{sd2_{30}}$	V_{g30}	V_{x30}	V_{y30}	J_{max30}	J_{min30}	J_{r30}	Φ_{30}
Pearson Correlation	A	0.09	0.18	0.67	0.15	0.48	0.05	0.00	0.00	0.50	0.49	0.09	0.00	0.65	0.17	0.00	0.07	0.00	0.06	0.51	0.49	0.12	0.00
	I	0.00	0.07	0.11	0.36	0.14	0.04	0.00	0.00	0.12	0.12	0.00	0.04	0.10	0.33	0.13	0.00	0.00	0.05	0.12	0.11	0.05	0.04
	V_x	0.00	0.00	0.10	0.02	0.04	0.16	0.21	0.00	0.08	0.00	0.00	0.03	0.09	0.00	0.00	0.18	0.28	0.00	0.09	0.00	0.00	0.00
	V_y	0.00	0.05	0.00	0.00	0.05	0.00	0.00	0.15	0.04	0.00	0.00	0.00	0.00	0.00	0.05	0.00	0.04	0.22	0.05	0.04	0.00	0.00
	Ltot	0.00	0.11	0.36	0.10	0.22	0.09	0.00	0.00	0.22	0.20	0.05	0.05	0.34	0.00	0.21	0.10	0.00	0.00	0.22	0.20	0.08	0.07
	Average	0.00	0.08	0.25	0.13	0.18	0.07	0.10	0.10	0.19	0.16	0.05	0.04	0.24	0.10	0.08	0.07	0.10	0.10	0.19	0.17	0.05	0.02
Partial Information Correlation	A	0.00	0.08	0.15	0.00	0.00	0.22	0.00	0.00	0.00	0.00	0.00	0.01	0.00	0.00	0.33	0.00	0.07	0.00	0.00	0.33	0.00	
	I	0.00	0.00	0.00	0.00	0.00	0.00	0.00	0.00	1.00	0.00	0.00	0.00	0.00	0.00	0.00	0.00	0.00	0.00	0.00	0.00	0.00	0.00
	V_x	0.00	0.00	0.00	0.00	0.00	0.00	0.00	0.00	0.00	0.00	0.00	0.00	0.00	0.00	0.00	0.00	1.00	0.00	0.00	0.00	0.00	0.00
	V_y	0.00	0.00	0.00	0.00	0.00	0.00	0.00	0.00	0.00	0.00	0.00	0.00	0.00	0.00	0.00	0.00	0.00	0.00	1.00	0.00	0.00	0.00
	Ltot	0.00	0.15	0.13	0.00	0.00	0.24	0.00	0.00	0.00	0.00	0.00	0.00	0.00	0.00	0.00	0.33	0.00	0.00	0.00	0.11	0.33	0.00
	Average	0.00	0.05	0.06	0.00	0.00	0.09	0.00	0.00	0.20	0.00	0.00	0.00	0.00	0.00	0.00	0.13	0.20	0.01	0.20	0.02	0.13	0.00

436 The application of the PIC analyses requires that the most important predictors should be introduced to the
 437 analysis first. Hence based on the Pearson correlation values from **Table 3** the following most important predictors were
 438 selected: Area –A (as maximum correlation value from first row), Intensity – PI_{sd1} (as maximum correlation value from
 439 second row), - Velocity X – V_{x30} (as maximum correlation value from third row), Velocity Y – V_{y30} (as maximum
 440 correlation value from fourth row), Total Lifetime – A (as maximum correlation value from fifth row). The results of the
 441 PIC analysis are shown in the lower row of **Table 3** and **Appendix 11.2**. For storm duration lower than 3 hours, where a
 442 lot of zeros are present, the PIC methods seems to be unable to converge to stable results or to identify important predictors.
 443 For the intensity and velocity components, the PIC identifies only 1 important predictor which, in the case of the Intensity
 444 and Velocity in the Y direction, does not correspond with the most important predictor fed first in the analysis. Contrary

445 for Total Lifetime and Area, only for storms that last longer than 3 hours, the method is able to converge and give the
 446 most important predictors; for Area - A, V_g , past V_{y30} and the L_{now} , while for Total Lifetime - A, Vel_g , L_{now} and $Jmin_{30}$. At
 447 the moment it is unclear why the PIC method is unable to perform well for all of the target variables and storm groups.
 448 One reason might be that only the Area and Total Lifetime are dependent on the chosen target variables. Another most
 449 probable reason might be that for the other target variables the heavy-tail of the probability distribution and the high zero
 450 sample size may influence the calculation of the joint and mutual probability distribution. The Total Lifetime is an easier
 451 target to be analysed, which means the values are not zero and its distribution is not as heavy tailed as the distribution of
 452 the other variables. The other variables, depending on the lead time, have more zeros included and have an asymptotic
 453 density function. It seems that, whenever zeros are not present, like in the case of storms lasting longer than 3 hours, the
 454 PIC is able to represent quite well the important predictors. However, the reason why this method is performing poorly
 455 for the application at hand, even though developed specifically for the k-NN application, is not completely understood
 456 and is not investigated further on for the time being since it is outside the scope of this paper.

457 Overall, the results from the Pearson correlation seem more robust and stable (throughout the lead times and
 458 storm groups) than the PIC method (refer to **Appendix 11.1** and **11.2**); the importance weights increase with the lifetime
 459 of the storm and decrease with higher lead time. These behaviours are expected as with increasing lead time the
 460 uncertainty becomes bigger and with increasing lifetime the storm dynamic becomes more persistent (due to the large
 461 scales and the stratiform movements involved). Moreover, the important predictors do not change drastically from one
 462 lead time or storm group to the other, as seen in the PIC. Therefore, the predictors estimated from the correlation with the
 463 given weights in **Table 3** are used as input to the k-NN application. In order to make sure that the predictor set from the
 464 Pearson correlation was the right one, the improvement in the single k-NN training error of using these predictors instead
 465 of the ones from PIC are shown in **Figure 7**. The results shown in this figure are computed according to the Equation (11)
 466 (where “new” is k-NN with correlation weights, and “ref” is the k-NN with PIC weights) for the target-based k-NN
 467 approach (solid lines) and storm-based k-NN approach (dashed lines) and are averaged for three groups of nowcast times
 468 as indicated in the optimization of k-NN (Section 3.2.3) and as well in the legend of **Figure 7**.

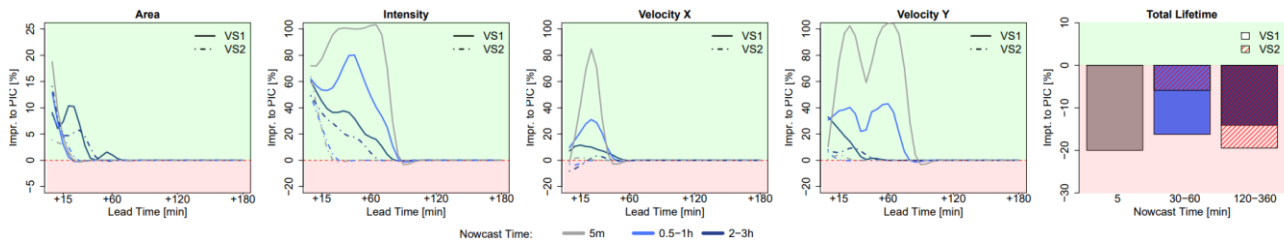


Figure 7 The median Mean Absolute Error (MAE) improvement per lead time and target variable from applying the k-NN (VS1 target-based, VS2 storm-based) with the predictors and weights derived by the Pearson correlation instead of PIC. The improvements are averaged for different times of nowcast. The green plot region indicates a positive improvement of the correlation predictors in comparison to the PIC, and the red region indicates a deterioration.

469 The results from **Figure 7** indicate that for the Area, Intensity, and Velocity components, the Pearson correlation
 470 weights improve the performance of target-based k-NN from 5 up to 100% compared to the PIC weights. This happens
 471 mainly for the short lead times ($LT < +60$ min) throughout the three groups of nowcast times. For longer lead times there
 472 seems to be no significant difference between the predictors sets. The same cannot be said for the Total Lifetime as a
 473 target variable, here the Pearson correlation weights do not give the best results for all the nowcast times. In fact, here the
 474 k-NNs based on the PIC weights seem to be more appropriate and yielded better results. However, as the other 4 target
 475 variables are better for the Pearson correlation, this predictor set was selected for all applications of the k-NN (with
 476 different weights according to **Table 3**) to keep the results consistent with one another. A further analysis was done that

477 proved that the application of the correlation weights produces lower errors than the non-weighted k-NN application (all
 478 weights are assigned to 1 to the most important predictors from Pearson correlation).

479 Lastly, it should be emphasized that for the computation of predictors weights, all the events were grouped
 480 together, and thus when applying the k-NN nowcast in the cross-validation mode, there is a potential that the information
 481 leaks from the importance analysis to the performance of the k-NN (also illustrated in **Figure 3-c**). In other words, the
 482 performance of the k-NN will be better, because the weights were derived from all the events grouped together. Typically,
 483 in modelling applications, the optimization dataset should be clearly separated by the validating one, in order to remove
 484 the effect of such information leakage. For this purpose, the correlation weights were computed 110 times, on a “leave-
 485 one-event-out” cross-sampling, in order to investigate their dependence on the event database. The results of such cross-
 486 sampling are visualized in **Appendix 11.3** and indicate a very low deviation of the predictors weights (lower than 0.01)
 487 over all the target variables. The shown low variability of the Pearson Correlation weights justifies the decision to estimate
 488 the weights from the whole database, as the potential information leakage is not likely affecting the results of the k-NN
 489 performance. This is another reason favouring the calculation of the predictor’s weights based on the Pearson Correlation.
 490 On the other hand, the weights from the PIC analysis are changing very drastically depending on the dataset and hence
 491 the effect of the information leakage would be much larger in the k-NN developed from PIC weights. Moreover, a
 492 sensitivity analysis as done in **Appendix 11.3** cannot be performed for the PIC analysis because it would be extremely
 493 time consuming.

494 4.2 Optimizing the deterministic k-NN nowcast

495 Once the most important predictors and their weights are determined, the optimization of the single k-NN
 496 nowcast for the two k-NN applications (storm-based and target-based) was performed. The optimal k-value obtained from
 497 minimizing the mean absolute error (MAE) produced by k-NN are shown in **Figure 8-upper row**. The results are
 498 computed for the given nowcast times, lead times and target variables for both k-NN applications (VS1 target-based and
 499 VS2 storm-based). For the 4 target variables Area, Intensity and Velocity in X/Y direction, the number of optimal values
 500 decreases quasi exponentially for lead time up to 1 hour. After these lead time, when the majority of the storms are

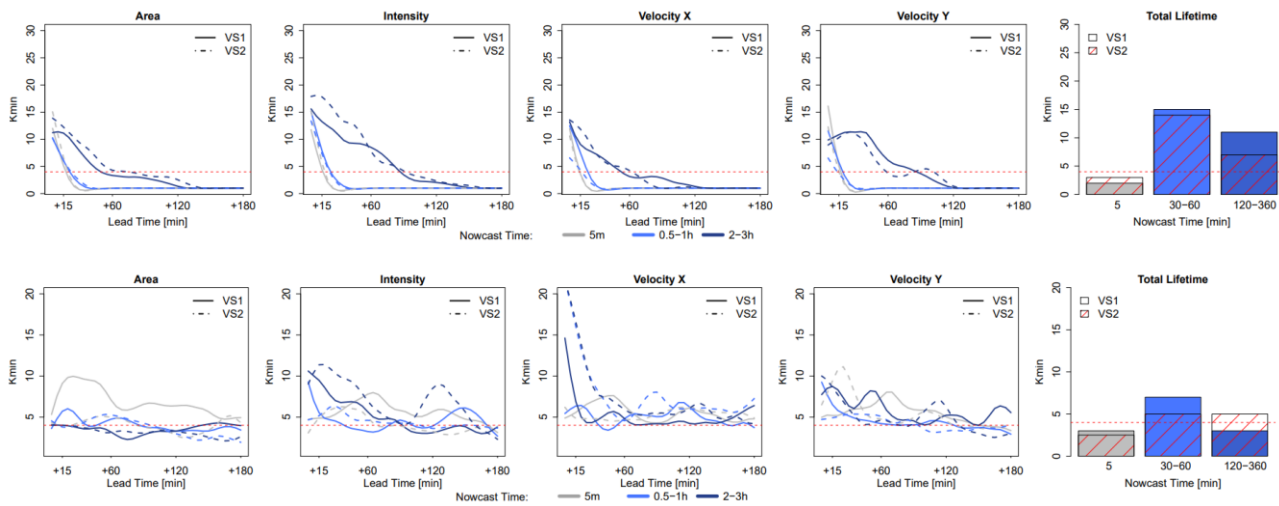


Figure 8 The optimization of the k-NN per target variable based on predictors and weights derived from Pearson correlation analysis: the median optimal selected “k” neighbours yielding the lowest absolute errors over the 110 events. Two k-NN applications are shown here – VS1 in solid line and VS2 in dashed line: first row – The optimal neighbour is found from minimizing the MAE for given group of nowcast times per event, second row – The optimal neighbour is found from minimizing the absolute mean error (ME) for the given group of nowcast times per event. The red dashed horizontal line indicates the k=4 that is chosen in this study for the deterministic k-NN application.

501 dissipated, the optimal k-number converges at 1, meaning that the closest neighbour is enough to predict the dissipation
502 of the storms. Contrary, for the very short lead times, the closest identified neighbour is unable to capture the growth/decay
503 processes of the storms, thus the response has to be average from k-neighbours, with k depending strongly on target
504 variable, nowcast time, lead time, and total lifetime. This seems to be the case also for the Total Lifetime, where averages
505 between 3-15 neighbours are computed as K_{min} . Overall the $k=1$ seems to yield the lowest MAE for the majority of the
506 lead time, nowcast times and target variables, and therefore is selected to continue further on with the analyses. However,
507 selecting the first neighbour does not satisfy the requirement that the nature doesn't repeat itself, and ideally a $k>1$ should
508 be achieved such that the responses from similar neighbour can be averaged to create a new response. For this purpose,
509 the optimal K were additionally obtained by minimizing the absolute mean error (ME) and are shown in **Figure 8 -lower**
510 **row**. Here the overestimation and underestimation of different storms balance one another, and the results seem to
511 converge when averaging 3-5 neighbours. A direct comparison of the MAE for $k=2-5$ and $k=1$ was performed in order to
512 understand if a higher k will benefit the application of both k-NN versions. The median improvements of using neighbours
513 from 2-5 instead of 1 (over the selected groups of nowcast times) are shown only for the Total Lifetime in **Table 4**. The
514 other target variables are left outside this analysis as the improvements averaged over all the lead times are very close to
515 zero, as the dissipation of storms is captured well by all the 5 closest neighbours. From the results of the **Table 4** it is
516 visible that $k=4$ brings the most advantages and hence was selected for both applications as a better compromise. The
517 selection of $k=4$ is not an optimization per se, as it was not learned with artificial intelligence, instead was selected based
518 on human intuition, and it does not represent the best possible training of the K_{min} . For a more complex optimization, the
519 machine learning can be employed in the future to learn the parameters of the exponential relationship between K_{min} , lead
520 time, nowcast time and target variable. In that case a proper splitting of the database into training and validation should
521 be done in order to avoid, information being leaked from the optimization to the validation of the k-NN. In our case, the
522 effect of the information leakage at this stage (also illustrated in **Figure 3-c**) is minimized by obtaining the K_{min} on a
523 cross-sampling of the events, and averaged over the events, lead times and nowcast times.

Table 4 The median improvement of the total lifetime MAE when using $k= 2- 5$ instead of $k=1$ over the three selected groups of nowcast times.

	k=2	k=3	k=4	k=5
Storm-based	9.09%	10.74%	13.09%	11.94%
Target-based	3.40%	5.89%	6.54%	6.02%

524

525 **4.3 Results of the deterministic 4-NN nowcast**

526 The median MAE of the 4-NN deterministic nowcast over all the events, run for both target- and storm-based
 527 approaches are shown in **Figure 9** for each lead time and target variable. The results are grouped according to the storm
 528 duration; i) upper row – for storms that live 30min, ii) middle row – for storms that live up to 3 hours and iii) lower row
 529 – for storms that live longer than 3 hours, and are averaged per nowcast times given in **Table 2**. As shown as well in the
 530 optimization of the 4-NN, the target-based k-NN exhibits lower Area, Intensity and Velocity errors than the storm-based
 531 4-NN. **Table 5-a** illustrates the median deterioration (-) or improvement (+) in percent (%) over all lead times that the
 532 storm-based 4-NN can reach when compared to the target-based one.

Table 5 Median Deterioration (-) or Improvement (+) of k-NN storm-based (VS2) compared to target-based (VS1) over all lead times according to the storm duration and nowcast times (shown in %). Equation 11 is used here, where “ref” – is the target-based and “new” is the storm-based k-NN.

a) deterministic comparison of median MAE from storm-based to target - based																																																		
Storm Duration	Nowcast Time						Storm Duration	Nowcast Time						Storm Duration	Nowcast Time																																			
	5min	15min	30min	Area	Intensity	Total Lifetime		5min	15min	30min	Area	Intensity	Total Lifetime		5min	15min	30min	Area	Intensity	Total Lifetime																														
30min	5min	-3%	8%	-8%	-27%	2%	0.5-3h	5min	-0.21%	-2%	3%	-1%	-4%	>3h	5min	-9%	0%	2%	-1%	-1%	15min	0%	7%	-14%	-38%	-7%	60min	30.00%	2%	-5%	23%	-11%	120min	-10%	-7%	-3%	-10%	2%	180min	-15%	-28%	-100%	-100%	28%	360min	-10%	-8%	-8%	21%	18%
	b) probabilistic comparison of median MAE from storm-based to target - based																																																	
	Storm Duration	Nowcast Time						Storm Duration	Nowcast Time						Storm Duration	Nowcast Time																																		
5min		15min	30min	Area	Intensity	Total Lifetime	5min		15min	30min	Area	Intensity	Total Lifetime	5min		15min	30min	Area	Intensity	Total Lifetime																														
30min	5min	-19%	7%	-12.75%	-50.00%	0.50%	0.5-3h	5min	-3.00%	0.00%	-0.50%	-14.40%	-4.02%	>3h	5min	-9.30%	-4.24%	1.10%	-0.67%	-9.27%	15min	3%	4%	-6.95%	-58%	-9.61%	60min	11.58%	-0.23%	-11.60%	15.37%	3%	120min	-5%	2%	-4%	-5%	4.79%	180min	-8%	-4%	-100%	-88%	5%	360min	-3.50%	-0.42%	-16%	11%	5.14%
	c) deterministic comparison of median improvement towards Langrangean Persistence from storm-based to target-based																																																	
	Storm Duration	Nowcast Time						Storm Duration	Nowcast Time						Storm Duration	Nowcast Time																																		
5min		15min	30min	Area	Intensity	Total Lifetime	5min		15min	30min	Area	Intensity	Total Lifetime	5min		15min	30min	Area	Intensity	Total Lifetime																														
30min	5min	-1%	0%	0%	-1%	0%	0.5-3h	5min	0.00%	0%	1%	0%	>3h	5min	-26%	0%	6%	-8%	15min	0%	0%	0%	-1%	0%	60min	12.53%	1%	-1%	3%	0%	120min	-31%	-22%	-29%	-39%	0%	180min	0%	0%	1%	0%	0%	360min	-5%	-21%	-8%	89%	0%		
	d) probabilistic comparison of median improvement towards Langrangean Persistence from storm-based to target-based																																																	
	Storm Duration	Nowcast Time						Storm Duration	Nowcast Time						Storm Duration	Nowcast Time																																		
5min		15min	30min	Area	Intensity	Total Lifetime	5min		15min	30min	Area	Intensity	Total Lifetime	5min		15min	30min	Area	Intensity	Total Lifetime																														
30min	5min	-1%	0%	0%	0%	0%	0.5-3h	5min	-1.40%	0%	0%	-1%	>3h	5min	-44%	-11%	5%	-3%	15min	0%	0%	0%	0%	0%	60min	2.50%	0%	0%	0%	0%	120min	-20%	11%	-5%	-6%	0%	180min	-1%	0%	0%	-1%	0%	360min	-8%	0%	-24%	6%	0%		

533 For storm living less than 30 minutes, the MAE is decreasing with the lead time and past LT+30 min is mostly
 534 zero, as the dissipations of the storms have been captured successfully. The Total Lifetime of the majority of the storms
 535 can be captured with ~ 15 min over-/underestimation regardless of the nowcast time. The errors for the 4 target variables
 536 (except Total Lifetime) are lower for the later nowcast times than for the earlier ones (as expected). The difference between
 537 the storm- and target-based 4-NN is very small for Area, Intensity and Total Lifetime, but much higher for the velocity
 538 components (with storm-based exhibiting up to 40% higher errors than the target-based). The biggest difference seems to
 539 be for shorter lead times (LT < +1h). For the storms living up to three hours, the same behaviour is, more or less, observed.
 540 The only difference is for nowcasts issued at 3rd hour of the storm existence (last moment the storm is observed). Here it
 541 is clear that the 4-NN fails to capture the dissipation of the storms that live exactly three hours, however this is attributed
 542 to the number of available storms with duration of 3 hours (median over 6 storms available). Since the Area, Intensity and
 543 Total Lifetime are overestimated and not converging to zero for high lead times, it is clear that the nearest neighbours are
 544 being selected from the longer storms that do not dissipate within the next 3 hours. The differences between the two 4-
 545 NN approaches are visible mainly for lead times up to 30 min (except the nowcast at 3rd hour of storms life), afterwards
 546 the errors are relatively converging to each other. The storm-based 4-NN produces circa 10-20% higher errors than the
 547 target-based one for the nowcast times lower than 3hours, while for nowcast time of 3 hours, the errors are up to 100%
 548 higher than the target- based one. At these storms as well, the higher discrepancy between the two versions of 4-NN is
 549 seen at the Velocity components.

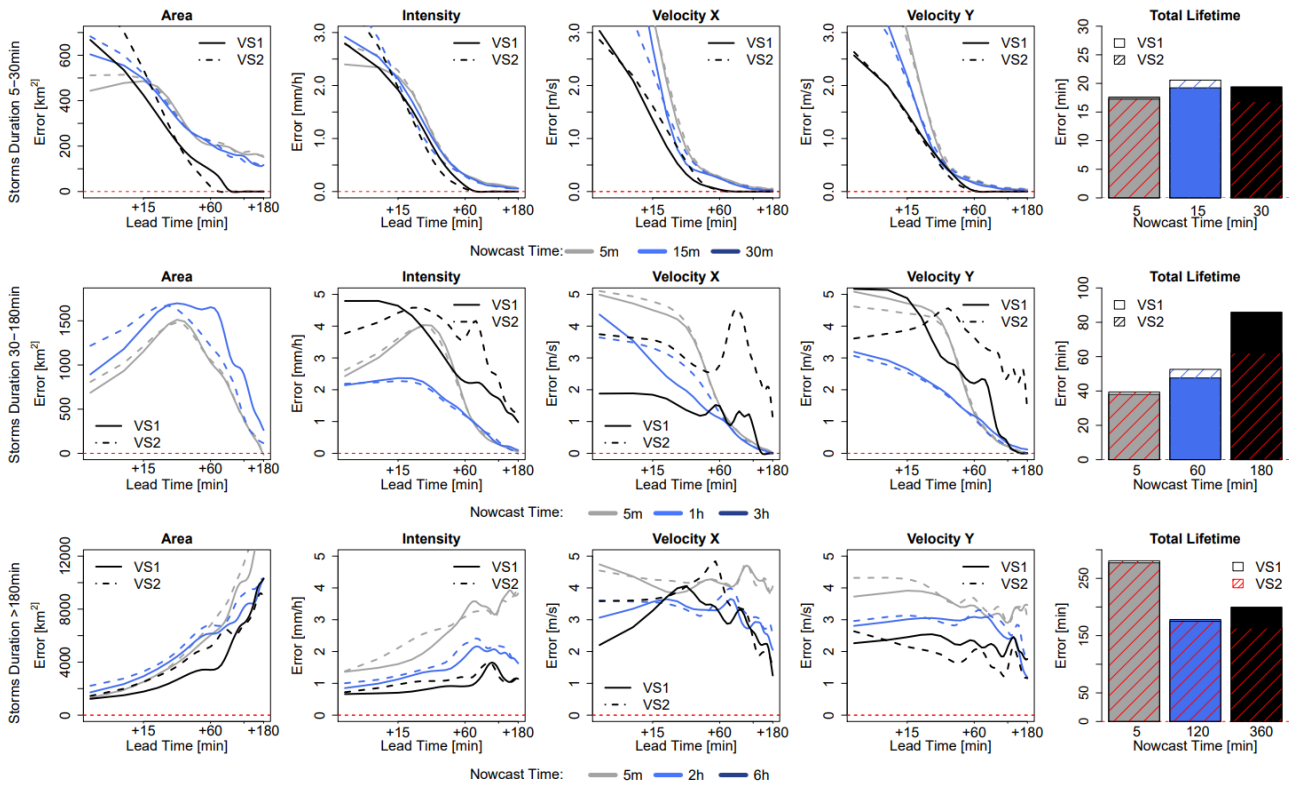


Figure 9 The median mean absolute error (MAE) over all the events, for each target variable (Area, Intensity, Velocity in X and Y direction and Total Lifetime) based on two 4-NN applications: -VS1 in solid and VS2 in dashed lines. The performance is shown for storms that are: shorter than 30 min (upper row), than 3 hours (middle row), and longer than 3 hours (lower row), and over the selected nowcast times. Nowcast time dictates when the nowcast is issued relative to storm initiation

550 For the storms that live longer than 3 hours (under 100 storms available) the same problem, as in the nowcast
 551 time of 3 hours seen before, is present. The Total Lifetime is clearly underestimated (up to 100min) as due to database the
 552 information is taken from shorter storms. It is important to notice here, that although 70 storms are present, because of
 553 the “leave-one-event-out” validation, the storm database is actually smaller. Nevertheless, the error is manifested here
 554 differently: as the long storms are more persistent in their features: Area, Intensity and Velocity components are captured
 555 better for the short lead times with the error increasing at higher lead times. Here as well the nowcast issued at the earlier
 556 stages of the storm’s life exhibit higher errors than in the later stages. Especially for the nowcast at the 6th hour of the
 557 storm’s existence, the errors are quite low for all 5 target variables due to the persistence of the stratiform storms. For this
 558 group of long storms, the storm-based nowcast yields up to 10% higher errors than the target-based one, with only few
 559 exceptions depending on the time of nowcast and variable. It is clear that the storm-based 4-NN is more influenced by
 560 the number of available storms than the target-based approach.

561 **Figure 10** shows the improvement that the 4-NN introduces to the nowcast when compared to the Lagrangian
 562 persistence (either target- or storm-based) and are averaged per lead time for each of the three group of storms and the
 563 respective times of nowcast. Since the Lagrangian Persistence doesn’t issue a Total Lifetime nowcast, only the four target
 564 variables (Area, Intensity and Velocity components) are considered. The green area indicates the percent of improvement
 565 from the application of the 4-NN approach, and the red area indicates the percent of deterioration from the 4-NN
 566 application (Lagrangian persistence is better). Additionally, median improvements (+) or deterioration (-) over all lead
 567 times of the storm-based compared to target-based 4-NN approach in respect to the Lagrangian Persistence are illustrated
 568 in **Table 5-c**. For the 30min storms, the 4-NN approach (both target- and storm-based) are considerably better than the

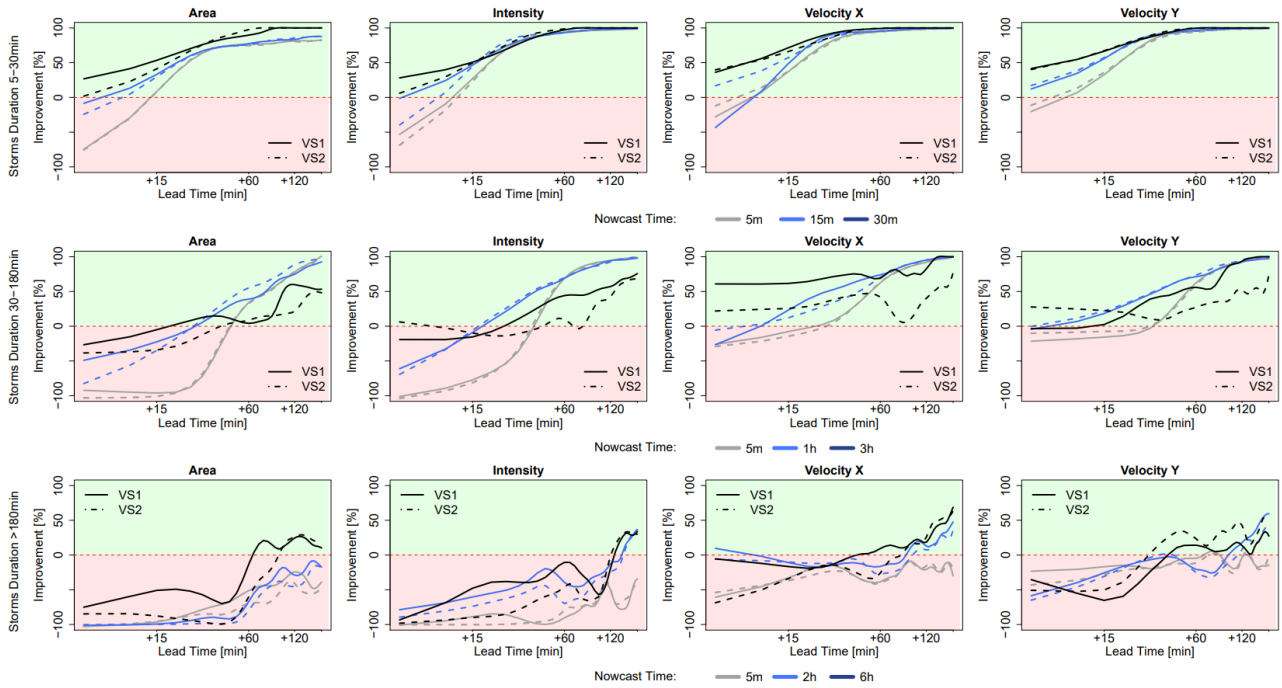


Figure 10 The median improvements over all the events that the single 4-NN application can introduce in the nowcast of the target variables (Area, Intensity, Velocity in X and Y direction) in comparison to the Lagrangian persistence. The results are shown for each 4-NN application: VS1 in solid and VS2 in dashed lines and are calculated separately for storms that live shorter than 30 min (upper row), shorter than 3 hours (middle row) and longer than 3 hours (lower row), and for the respective nowcast times. The green region of the plot indicates a positive improvement (better nowcast by the 4-NN application) and the red region indicates a deterioration (better nowcast by the Lagrangian persistence).

569 Lagrangian persistence: improvement is higher than 50% from the LT+15min and up to 100% from LT+60min. The
 570 improvement is greater for nowcast at the 15th min of storm existence (when the persistence predictors are considered). It
 571 is clear than due to the autocorrelation, the Lagrangian persistence is more reliable for the short lead times and for earlier
 572 nowcast times. However, after LT+15min and for nowcast times near to the dissipation of the storms, where the non-
 573 linear relationships govern, the improvements from the nearest neighbour are more significant. The target-based 4-NN
 574 results in slightly higher improvements than the storm-based one only for lead time up to 30min, past this lead time the
 575 improvements from both versions are converging. For the storms that live between 30 min to 3 hours, the improvements
 576 are introduced first after LT+15 or +30 min depending on the nowcast time: with increasing nowcast time increases the
 577 improvement as well. The only exception is for the nowcast of Area and Intensity on the 3rd hour of the storm existence,
 578 where no clear improvement of the 4-NN approaches could be seen before LT+30min or LT+1h. This low improvement
 579 for the nowcast time of 3 hours was expected following the poor performance of the 4-NN shown in **Figure 9**. It seems
 580 like the Lagrangian persistence is particularly good for predicting the Area and Intensity at very short lead times (up to
 581 LT+20min). Here, for nowcast times of 5min, the Lagrangian Persistence is 100% better than any of the 4-NN approaches.
 582 But not the same is true for the Velocity Components, with the Lagrangian Persistence exhibiting very low advantages
 583 against the 4-NN for the short lead times. Regarding the difference of the two 4-NN approaches, with few exceptions, the
 584 storm-based nowcast exhibits similar improvements as the target-based. Another exception is the nowcast time of 3 hours,
 585 where the storm-based improvements are clearly lower, especially for the higher lead times, than the target-based (up to
 586 40%). For storms living longer than 3 hours, the improvements are present for lead times higher than 2 hours. Since the
 587 features of the long storms (mostly of stratiform nature) are persistent in time, is understandable for the Lagrangian

588 Persistence to deliver better nowcast up to LT+2h. Past this lead time non-linear transformations should be considered.
589 Here, even though the storm database is small, the non-linear predictions based on the 4-NN capture better these
590 transformations than the persistence. The improvement introduced by the storm-based are generally from 20-30% lower
591 than the improvements introduced from the target based.

592 To conclude, the 4-NN deterministic nowcast brings up to 100% improvements for lead times higher than the
593 predictability limit of the Lagrangian persistence and depend mainly on the storm type and the size of database. Overall,
594 for all storms the improvement is mainly at the high lead times and later times of nowcast, as the 4-NN is capturing
595 particularly well the dissipation of the storms. The results from the long events are suffering the most from the small size
596 of the database. This was anticipated, as the events were mainly selected from convective events that have the potential
597 to cause urban floods. A bigger database, with more stratiform events included, can introduce a higher improvement to
598 the Lagrangian persistence. These improvements are expected to be higher for lead times longer than 2 hours, but is yet
599 to be seen if a larger database can as well behave better than the persistence even for lead times shorter than the
600 predictability limit. Regarding the two different 4-NN approaches, the storm-based performs 0-40% worse than the target-
601 based nowcast, introducing generally 40% lower improvements to the Lagrangian persistence. The main differences
602 between these two approaches lie between the growth/decay processes, which the target-based 4-NN can capture better.
603 Also, these differences are particularly larger for the Velocity Components and for the Total Lifetime, than in the Area
604 and Intensity as target variables. Furthermore, it seems that the storm-based 4-NN is more susceptible to the size of the
605 database than the target-based one. Nevertheless, there are some cases where the storm-based behaves better than the
606 target-based nowcast (as illustrated with green in **Table 5 -a**) even though the target-based approach should be profiting
607 more from the selected predictors and their respective weights. A better optimized K_{\min} for each lead time and nowcast
608 time, may actually improve further on the results of both 4-NN versions, and give the advantages mainly to target-based
609 nowcast.

610 **4.4 Results of the ensemble 30-NN nowcast**

611 The median CRPS over all the events for the probabilistic 30NNs (in solid lines) together with the
612 median MAE for the deterministic 4-NN (in dashed lines), are illustrated respectively for storm-based approach in **Figure**
613 **11** and for target-based approach approaches in **Figure 12**. The results are shown as in the previous figures per each lead
614 time and target variable, for storms divided into 3 groups according to their duration and averaged depending on the time
615 of nowcast. Additionally, the median improvements (+) or deterioration (-) of storm-based CRPS values in comparison
616 with the target-based are given in **Table 5-b**. For the 30min long storms, the errors of the probabilistic nowcast are
617 typically lower than the single 4-NN nowcast for all the variables, lead times and nowcast times, independent of the
618 30NNs approach (either storm- or target-based). In contrast to the deterministic 4-NN, the probabilistic 30NNs
619 performance is very little dependent on the nowcast time (mainly for Area, Intensity and Total Lifetime). The storm-based
620 30NNs has up to 50% higher errors than the target-based, but on the other side can have up to 40% lower errors than the
621 target-based for nowcast times of 30min. This suggests that storms in this duration behave similarly and their dissipation
622 can be predicted adequately by the storm-based approach with more than 4 similar neighbours. For storms that live shorter
623 than 3 hours, the same performance is as well exhibited: the probabilistic 30NNs has lower errors than the deterministic
624 4-NN. The difference between the target- and storm-based nowcasts is within the range of the single 4-NN nowcast for
625 the first 4 target variables, with storm-based 30NNs having 15% higher errors in the first 30 min of the nowcast than the
626 target-based. For Intensity and the Total Lifetime, both of the 30NNs exhibit very similar errors for most of the nowcast
627 times. It is worth mentioning here, that for the nowcast at the 3rd hour of storms' existence the errors are much lower than
628 the single 4-NN nowcast. This proves that the most similar storms are within the 30 members, but not within the first 4
629 neighbours selected in the case of the single 4-NN nowcast. Due to the unrepresentativeness in the database, the errors of

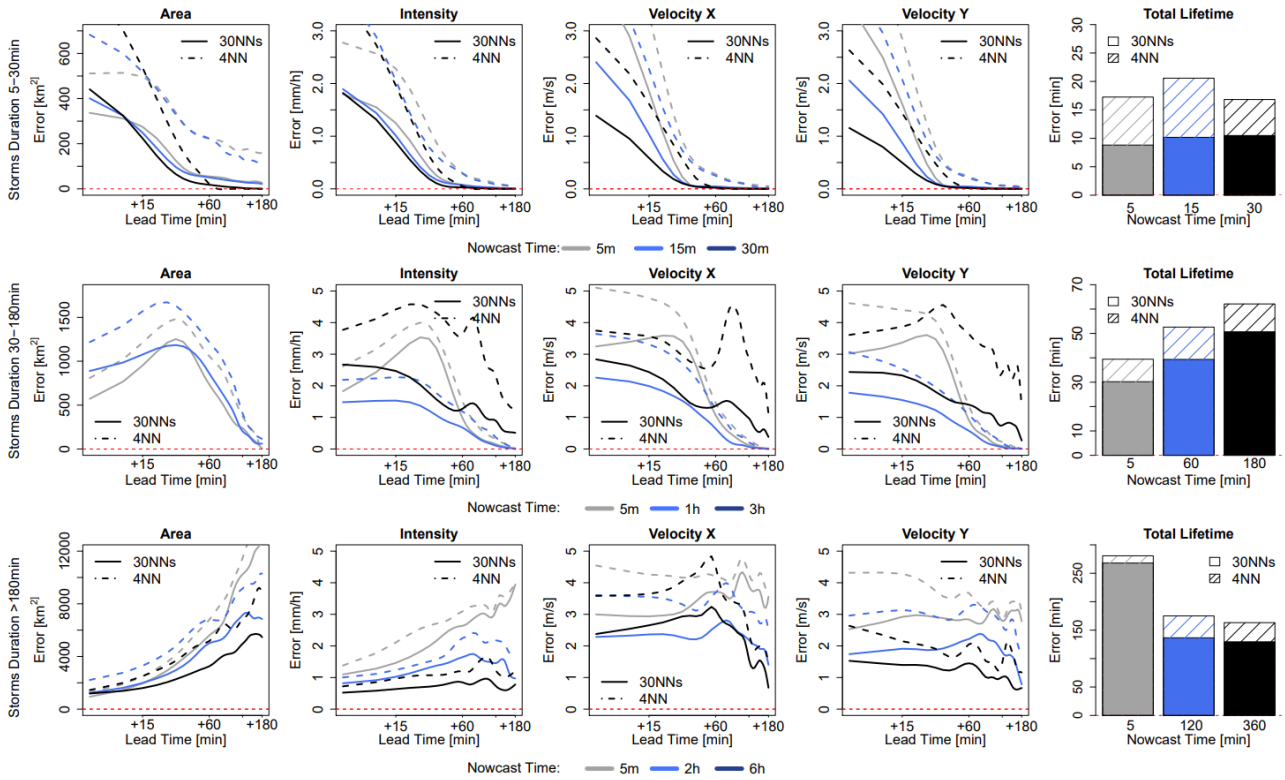


Figure 11 The median CRPS over all the events for each target variable (Area, Intensity, Velocity in X and Y direction and Total Lifetime) on the storm-based applications: 4-NN (deterministic) in dashed and 30NNs (probabilistic) in solid lines. The performance is computed over storms that are: shorter than 30 min (upper row), than 3 hours (middle row), and longer than 3 hours (lower row), and over the selected nowcast times.

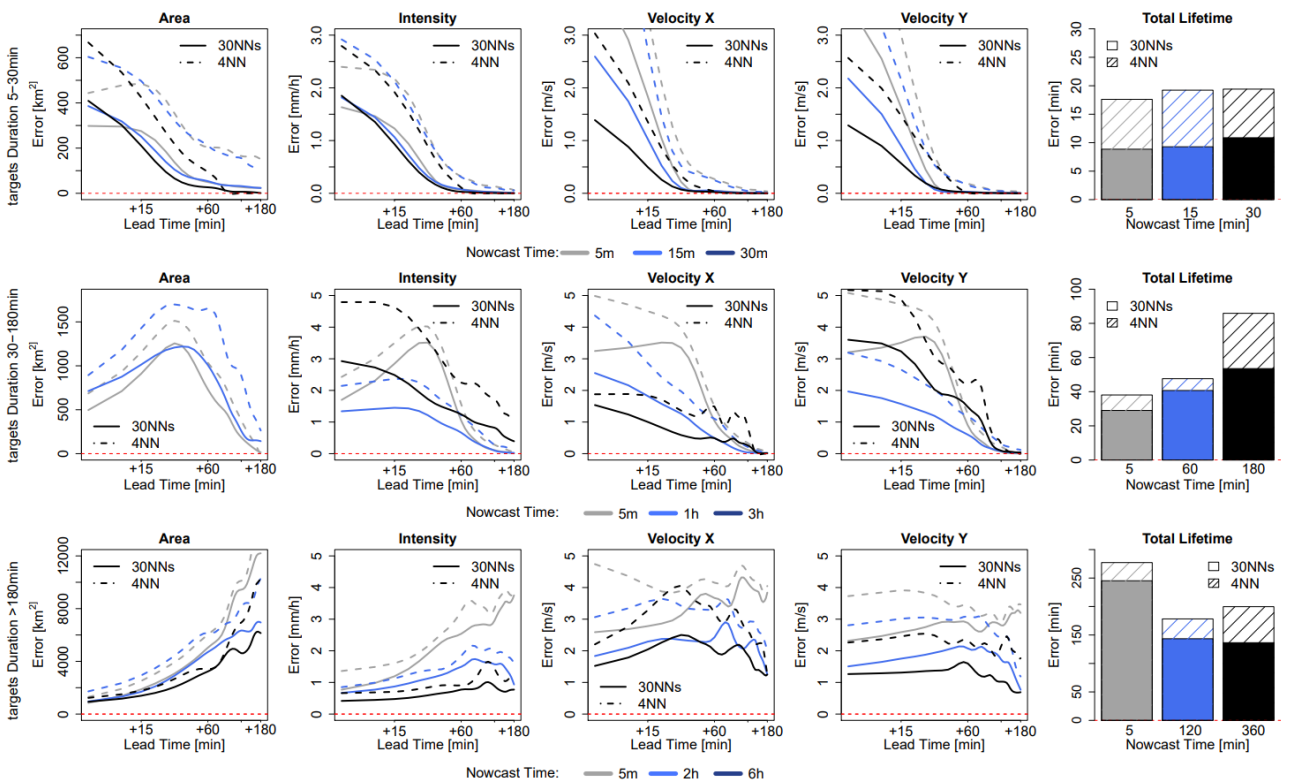


Figure 12 The median CRPS over all the events for each target variable (Area, Intensity, Velocity in X and Y direction and Total Lifetime) on the target-based applications: 4-NN (deterministic) in dashed and 30NNs (probabilistic) in solid lines. The median errors are computed over storms that are: shorter than 30 min (upper row), than 3 hours (middle row), and longer than 3 hours (lower row), and over the selected nowcast times.

631 the longer storms are considerably higher than the other storm groups, and the errors of the first 4 target variables are
 632 increasing with the lead time and decreasing with the nowcast time, as in the case of the deterministic 4-NN nowcasts.
 633 However here unlike the other storm groups, the differences between the storm-based and target-based approach are
 634 visible past 30 min lead time, with the storm-based errors being up to 15% higher than the target-based.

635 Overall the ensemble results are clearly better than the single 4-NN nowcast, suggesting that the best responses
 636 are obtained by singular neighbours (either the closest one or within the 30 neighbours) and not by averaging. Thus, there
 637 is still room for improving the single 4-NN nowcast by selecting better the important predictors and their weights or
 638 averaging differently the nearest neighbours. Nevertheless, the results from **Figure 11** and **Figure 12** emphasize that
 639 similar storms do behave similarly, and that the developed k-NN on the given database with 30 ensembles gives
 640 satisfactory results. Compared to the deterministic 4NNs it has the advantage that no k-optimization is needed, and the
 641 two approaches (storm- and target-based) have less discrepancies with one another.

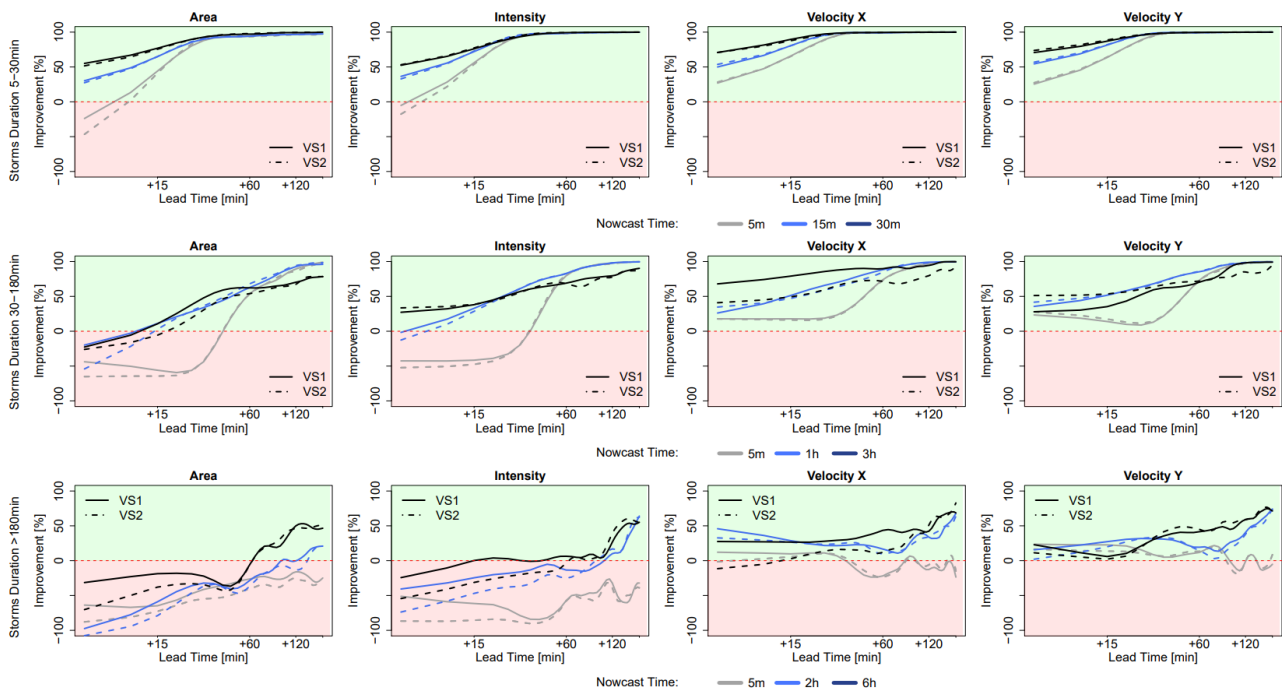


Figure 13 The median improvements over all events, that the 30NNs nowcast can introduce in the nowcast of the target variables (Area, Intensity, Velocity in X and Y direction) in comparison to the Lagrangian persistence. The results are shown for each 30NNs application: VS1 in solid and VS2 in dashed lines and are calculated separately for storms that live shorter than 30 min (upper row), shorter than 3 hours (middle row) and longer than 3 hours (lower row), and for the respective nowcast times. The green region of the plot indicates a positive improvement (better nowcast by the 4-NN application) and the red region indicates a deterioration (better nowcast by the Lagrangian persistence).

642 **Figure 13** demonstrates the improvement of the probabilistic 30NNs when compared to the Lagrangian
 643 persistence (storm-based in dashed line, and target-based in solid line). As before the median improvement over the events
 644 is computed and shown for each storm duration group, nowcast time, lead time and target variables (except for the Total
 645 Lifetime). For all the three groups it is visible that performance increases considerably with the lead time – suggesting
 646 that the ensemble predictions are particularly useful for the longer lead times where the single nowcast is not able to
 647 capture the storm evolution. For short storms (duration shorter than 30min) the Lagrangian persistence is only better for
 648 the Area and Intensity at 5min nowcast time and for very short lead times (up to 10min). However, past this lead time,
 649 the probabilistic 30NNs has the clear advantage with improvements up to 100%. Past LT+30min, which coincides with
 650 the predictability limit of the Lagrangian persistence at such scales, there is no difference between the nowcast time and

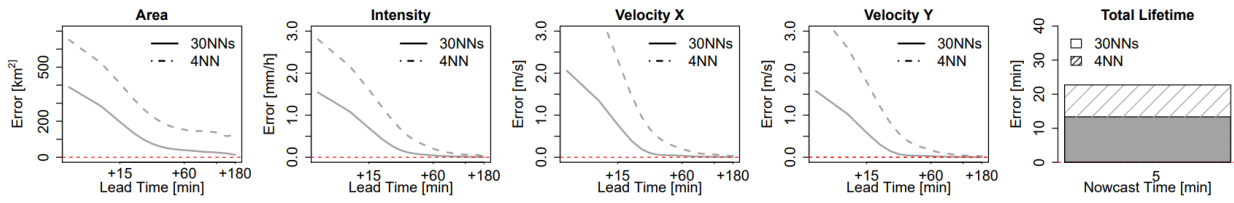
651 30NNs approach (less than 1% for all target variables and nowcast times). For storms that live shorter than 3 hours, the
652 results are slightly worse than the very short storms., but still exhibit the same patterns. Here as well the main
653 improvements of the 30NNs probabilistic approach is seen between LT+15min to LT+30min for all the target variables.
654 Interesting in this storm group are the results from the nowcast time of 3 hours that exhibit different behaviours than the
655 deterministic approach. This is expected as the Lagrangian persistence performs particularly poorly because it cannot
656 model the storms dissipations. The difference between the two types of 30-NN is insignificant, although a bit higher than
657 for the very short storms (~2.5% difference). For the longer storms the benefit of the probabilistic 30NNs is seen mainly
658 for LT+60min to LT+120min, but still not as high as in the other storm groups. The worse performance is at nowcast time
659 of 5min, where the 30NNs fails to bring any advantage to the prediction of Area and Intensity when compared to the
660 Lagrangian Persistence. Interesting from these storms, is that the improvement is more significant at the Velocity
661 Components than in the Area and Intensity predictions. This suggest the velocity components are more persistent (see
662 **Figure 4**) and easier to be predicted from similar storms.

663 As a conclusion the probabilistic nowcasts are better than the Lagrangian Persistence mainly for convective
664 storms that last shorter than 3 hours and lead times higher than LT+15min. Of course, there is still room for improving
665 the 30NNs application by increasing the size of the past database. Overall, it seems that the velocity components can be
666 captured much better by the 30NNs application than the Lagrangian Persistence, while the Lagrangian Persistence is more
667 suitable for long persistent storms and for nowcast times of 5min where not enough information is available to select
668 similar storms. An increase in the database, with more stratiform storms, may improve the performance of the 30NNs and
669 its advantage over the Lagrangian Persistence. However, the value of the probabilistic 30NNs relies mainly in the
670 nowcasting of convective events. Moreover, the possibility of merging Lagrangian Persistence with a probabilistic 30NNs
671 approach should be explored and further investigated; the Lagrangian Persistence should be implemented for very short
672 lead times (up to 30min) and for the first nowcast times where the predictors are not enough to select similar past storms.

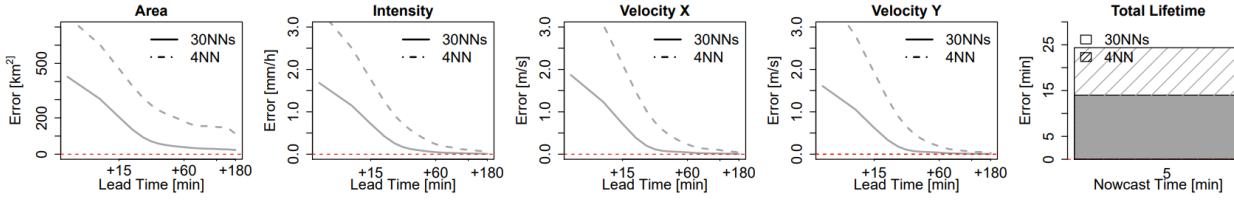
673 *4.5 Nowcasting the unmatched storms*

674 For the optimization and testing of the k-NN approaches, the unmatched storms from the tracking algorithm were
675 left outside of the database. Nevertheless, in an online application (operational nowcast), when the storm is recognized
676 for the first time, one cannot predict if the storm is an artefact, or it will not be matched by the tracking algorithm.
677 Therefore, it is important to investigate how the developed k-NN deals with these unmatched storms. **Figure 14** illustrates
678 the median performance over the 110 events of the developed target-based (upper row) and storm-based (lower row) k-
679 NN when predicting the target variables of the unmatched storms from a past database of only matched storms (storms
680 with duration equal or longer than 10min). As in the previous results, the 30NNs probabilistic application yields better
681 errors than the deterministic one, causing an overestimation of these storms for the first 10-20min for the target-based
682 approach and 15-30min for the storm-based one. A direct comparison of these errors with the Lagrangian Persistence is
683 shown in **Figure 15**, with the deterministic 4-NN in the upper row and the probabilistic 30NNs in the lower row. As
684 expected the probabilistic 30NNs brings the most improvement when compared to the Lagrangian Persistence for all lead
685 times and target variables. Thus, even though, most of these unmatched storms will be overestimated in their duration,
686 the 30NNs will capture their dissipation much better than either the deterministic 4-NN or the Lagrangian Persistence.

687

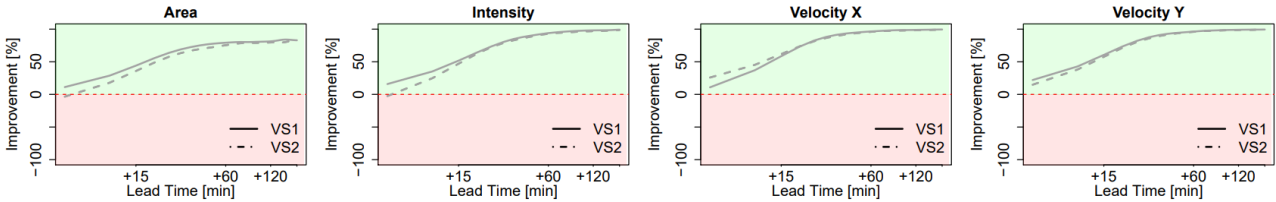


a) Target-based k-NN application

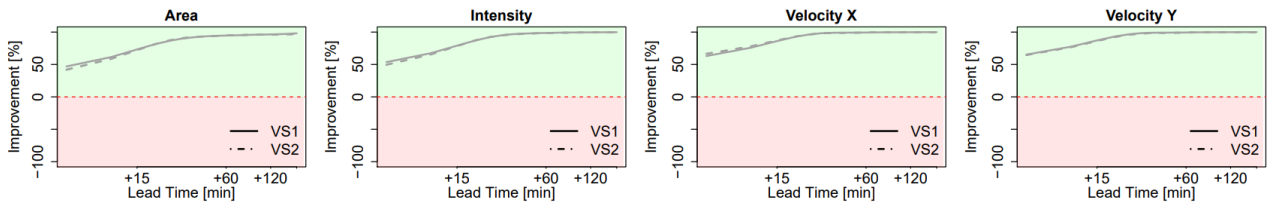


b) Storm-based k-NN application

Figure 14 Median CRPS error over the 110 events for each of the target variables nowcasted from 4-NN deterministic (in dashed lines) and 30NNs probabilistic (in solid lines) applications for both target- (upper row) and storm-based (lower row) approaches. The results shown here are from the “unmatched storms” when the nowcast time is 5 min.



a) deterministic 4-NN approach



b) probabilistic 30-NN approach

Figure 15 Median performance improvement over the 110 events for each of the target variables nowcasted from 4-NN deterministic (upper row) and 30NNs probabilistic (lower row) applications when compared to the Lagrangian Persistence, for both target- (dashed line) and storm-based (solid line) approaches. The results shown here are from the “unmatched storms” when nowcast time is 5 min.

688 5. Conclusions

689 Accurate predictions of rainfall storms at fine temporal and spatial scales (5min, 1km²) based on radar data are
690 quite challenging to achieve. The errors associated with the radar measurements, identification and tracking of the storms,
691 and more importantly the extrapolation of the storms in the future based on the Lagrangian persistence, are limiting the
692 forecast horizons of such object-oriented radar based nowcasts to 30-45 min for convective storms and to 1 hour for
693 stratiform events (Shehu & Haberlandt, 2021). The focus of this paper was the improvement of the storm-oriented radar
694 based nowcasts by considering other non-linear behaviours for future extrapolation instead of the Lagrangian persistence.
695 For this purpose, a nearest neighbour approach was proposed that predicts future behaviours based on past observed
696 behaviours of similar storms. The method was developed and validated for the Hannover Radar Range where storms from
697 110 events were pooled together and used in a “leave-one-event-out” cross-validation. From 110 events a total of around
698 5200 storms with different morphology were identified and tracked with HyRaTrac in order to build up the database for
699 the k-NN implementation. The storms were treated as ellipses and for each state of the storms’ evolution different features
700 (describing both present and past states) were computed. The k-NN approach was developed on these features to predict
701 the behaviour of the storms in the future (for lead times up to 3 hours) through 5 target variables (Area, Intensity, Velocity
702 in X and Y direction and Total Lifetime).

703 First an importance analysis was performed in order to recognize the most important predictors for each target
704 variable. Two different approaches were employed for this purpose: Pearson correlation, and Partial Information
705 Correlation (PIC). A comparison of these two methods revealed that for the application at hand the Pearson Correlation
706 is more reliable at determining important predictors, and delivers 5%-30% better results than the PIC method. However,
707 the PIC seems promising mainly for determining the most important predictors of the Area and Total Lifetime for storms
708 longer than 3 hours, and is still recommended for investigation in the future. The Area, Intensity and Total Lifetime of the
709 storms seem to be co-dependent on one another and on the features that describe their evolution. In particularly the
710 variance of the spatial intensity is an important predictor for the three of them. On the other hand, the velocity components
711 are dependent as well more on features that describe their evolution. Nevertheless, there is still a dependency of the area
712 and velocity components, and should be included when predicting each other mainly for long lead times.

713 The weights derived from the Pearson correlation were used for the similarity estimation of different storms
714 based on the Euclidian distance. Two k-NN approaches were developed on two similarity metrics: a) target-based
715 approach – similarity was computed for each target independently and indicates the best performance possible by the
716 given predictors and weights, and b) storm-based approach – similarity was computed for each storm keeping the
717 relationship between the target variables. For the two approaches a deterministic (averaging the 4 closest neighbours) and
718 a probabilistic (with 30 nearest neighbours) nowcast were issued for all of the storms in “leave-one-event-out” cross-
719 validation mode. In the deterministic nowcast the difference between the two remains mainly at short lead times (up to
720 30 min) and at the Velocity Components, with the storm-based results yielding up to 40% higher errors than the target-
721 based ones. However, at higher lead times the difference between the two became insignificant, as the dissipation
722 processes were captured well for the majority of the storms. The same behaviours were observed as well in the ensemble
723 nowcast, with target-based ensembles being slightly better than the storm-based nowcast. Overall the storm-based
724 approach seems reasonable for Area-Intensity and Total Lifetime, as they are co-dependent and their relationship should
725 be maintained for each storm, while target-based approach captures better the velocity components. A combination of
726 both approaches, may results in better nowcasting of storms’ characteristics.

727 To investigate what value each of the two k-NN approaches introduces to the nowcast, their errors (for both
728 deterministic and probabilistic nowcast) were compared to the errors produced by the Lagrangian persistence. For both
729 of the approaches the improvement was more than 50% for convective storms for lead times higher than 15 min, and for

730 mesoscale storms for lead times higher than 2 hours. The results were particularly good for the small convective storms
731 due to the high number of storms available in the database. For the mesoscale storms (with duration longer than 3 hours)
732 the improvements were not satisfactory due to the small sample size of such long storms. Increasing the sample size is
733 expected to improve the performance of the k-NN for these storms as well. However, when consulting the probabilistic
734 k-NN application it seems that, even for these storms and the given database, there are enough similar members in the 30
735 neighbours that are better than the Lagrangian persistence. This emphasizes that the probabilistic nowcast is less affected
736 by the sample size than the deterministic 4-NN. Moreover, the differences between the storm-based and target-based
737 approaches, become smaller in the probabilistic approach than the deterministic ones. Lastly, the optimization of the
738 adequate neighbours for the deterministic approach is far more complex than implemented here, but when issuing the
739 probabilistic nowcast there is no need to optimize the k – number. It is clear that the probabilistic application of the k-NN
740 outperforms the deterministic ones, and has more potential for future works.

741 Overall the results suggest that if the database is big enough, storms that behave similarly can be recognized by
742 their features, and their responses are useful in improving the nowcast up to 3 hours lead times. We recommend the use
743 of the nearest neighbour in a probabilistic application (30NNs) to capture better the storm characteristics at different lead
744 times. A merging with the Lagrangian Persistence for short lead times (up to 15min) and early nowcast times can be as
745 well implemented. Further improvements can be achieved if the predictors importance is estimated better (i.e. Monte
746 Carlo approach, or neural networks) or if additional predictors are included from other data sources like: cloud information
747 from satellite data, temperature, convective available potential energy (CAPE) and convective inhibition (CIN) from
748 Numerical Weather Prediction Models, lightning flash activity, additional measurements from Doppler or dual polarized
749 radar data (like phase shift, doppler velocity, vertical profile at different elevation angles), various geographical
750 information (as distance from heavy urbanized areas, mountains or water bodies) and so on. The main benefit of the
751 probabilistic 30NNs is mainly seen for convective events and creating new nowcasting rules based on the predicted storm
752 characteristics.

753 Improving the nowcasting of storm characteristics is the first step in improving rainfall nowcasting at fine
754 temporal and spatial scales. On a second step, the knowledge about the storm characteristics (as nowcasted by the 30NNs)
755 should be implemented on the spatial structure of the storms to estimate rainfall intensities at fine scales (1km² and 5min).
756 There are two options to deal with the spatial distribution of the rainfall intensities inside the storm region (which is so
757 far not treated in this study): 1. Increase/Reduce the area by the given nowcasted area (as target variable) for each lead
758 time, scale the average intensity with the nowcasted intensity, and move the position of the storm in the future with the
759 nowcasted velocity in x and y direction. 2. Take the spatial information of the selected neighbours, perform an
760 optimisation in space (such that present storm and the neighbour's storms locations match) and assign this spatial
761 information to the present storm for each lead time. The former is an extension of the target-based 30NNs, while the later
762 an extension of the storm-based 30NNs. So far, the comparison between these two versions, showed that the target-based
763 approach is better suited mainly to nowcast the velocity components, thus a merging of the two could also be reasonable:
764 the storm-based approach is used for nowcasting Area-Intensity-Total Lifetime (features that are co-dependent based on
765 the life cycle characteristics of convective storms), and the target-based approach for the nowcasting of the velocity
766 components. Future works (Part II – Local Intensities) will include the integration of the developed 30NNs application in
767 the object-oriented radar based nowcast to extend the rainfall predictability limit at fine spatial and temporal scales (1km²
768 and 5min). The main focus of the Part II is to investigate if the methodology applied here can introduce improvements as
769 well at the local scale, i.e. validation with the measurements from the rain gauge observations.

770

771 **6. Data Availability**

772 All data and R-codes can be provided by the corresponding authors upon request.

773 **7. Authors Contribution**

774 Study conception and design B.S, and U.H., methodology: B.S. and U.H., software and data collection: B.S.,
775 analysis and interpretation of results: B.S., writing-review and editing: B.S. and U.H., supervision and funding
776 acquisition: U.H.

777 **8. Competing Interest**

778 The authors declare that they have no conflict of interest.

779 **9. Funding**

780 This research was funded by the German Federal Ministry of Education and Research (BMBF) grant number
781 Förderkennzeichen 03G0846B.

782 **10. Acknowledgements**

783 The results presented in this study are part of the research project “Real-time prediction of pluvial floods and
784 induced water contamination in urban areas (EVUS)”, funded by the German Federal Ministry of Education and Research
785 (Bundesministerium für Bildung und Forschung BMBF) who are gratefully acknowledged. We are also thankful for the
786 provision and right to use the data from the German National Weather Service (Deutscher Wetterdienst DWD), the
787 HyRaTrac program from Dr. Stefan Krämer, and to the Open Access fund of Leibniz Universität Hannover for funding
788 the publication of this article. Lastly, we would like to acknowledge as well the useful comments from the three reviewers
789 Seppo Pulkkinen, Ruben Imhoff and Georgy Ayzel that have improved the final version of the manuscript.

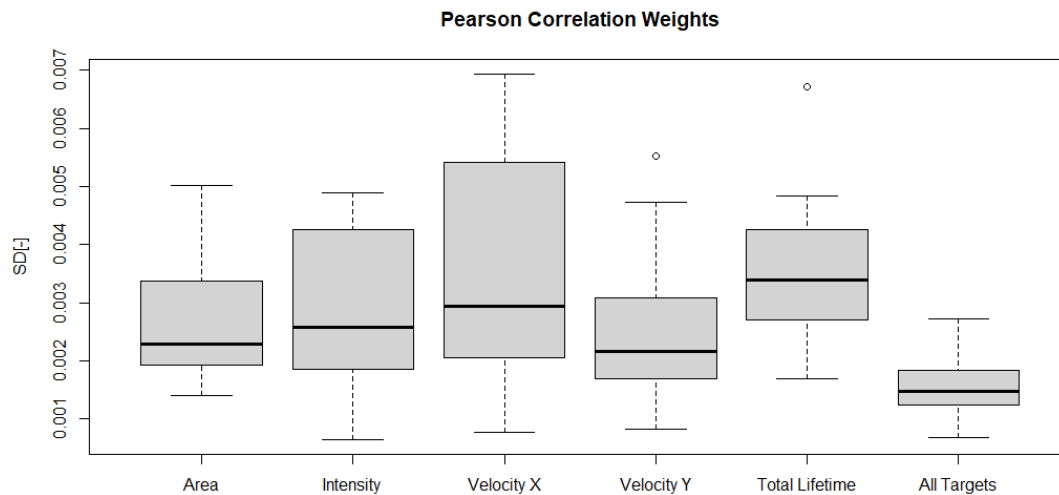
Appendix 11-1 Strength of relationship between the selected predictors and the target variables averaged for three lead times and storm duration groups based on correlation values. The green shade indicates the strength of the relationship: with 0 for no relationship at all, and 1 for highest dependency. The averaged computed values for each target variable (last row) are used as bases for Table 3. The correlation weights are absolute values of the correlation values between the predictors at specific lead times and target variables.

		Present Predictors														Average Past 30min Predictors													
Area	Durations Lead Time	Cells	Lnow	A	lave	lmax	lstd1	lstd2	Vg	Vx	Vy	Jmax	Jmin	Jr	Φ	A ₃₀	lave ₃₀	lmax ₃₀	lstd1 ₃₀	lstd2 ₃₀	Vg ₃₀	Vx ₃₀	Vy ₃₀	Jmax ₃₀	Jmin ₃₀	Jr ₃₀	Φ ₃₀		
		Area	<1hr	15min	0.19	0.22	0.81	0.06	0.05	0.05	0.59	0.06	0.02	0.01	0.58	0.61	0.01	0.00	0.79	0.06	0.05	0.05	0.61	0.06	0.02	0.02	0.60	0.62	0.01
60min	0.09			0.27	0.90	0.19	0.07	0.20	0.64	0.05	0.05	0.03	0.65	0.68	0.04	0.02	0.88	0.21	0.08	0.22	0.67	0.08	0.08	0.07	0.68	0.70	0.08	0.02	
180min	0.12			0.19	0.94	0.18	0.23	0.29	0.68	0.05	0.04	0.05	0.72	0.70	0.28	0.00	0.92	0.21	0.25	0.31	0.69	0.05	0.05	0.09	0.73	0.69	0.38	0.02	
<3hr	15min		0.12	0.19	0.61	0.04	0.03	0.04	0.45	0.00	0.01	0.00	0.43	0.49	0.01	0.01	0.60	0.05	0.02	0.04	0.46	0.00	0.02	0.02	0.45	0.50	0.01	0.01	
	60min		0.04	0.25	0.72	0.13	0.01	0.13	0.48	0.01	0.03	0.03	0.55	0.55	0.03	0.01	0.69	0.15	0.03	0.15	0.51	0.02	0.05	0.05	0.56	0.55	0.07	0.02	
	180min		0.09	0.13	0.80	0.16	0.20	0.25	0.58	0.10	0.01	0.05	0.63	0.57	0.24	0.00	0.77	0.20	0.23	0.28	0.57	0.11	0.00	0.09	0.61	0.55	0.32	0.02	
>3hr	15min		0.05	0.13	0.32	0.04	0.00	0.03	0.22	0.00	0.01	0.01	0.24	0.25	0.01	0.01	0.31	0.04	0.01	0.04	0.21	0.00	0.02	0.03	0.25	0.25	0.01	0.02	
	60min		0.03	0.14	0.42	0.13	0.09	0.14	0.27	0.07	0.02	0.02	0.32	0.26	0.02	0.02	0.39	0.15	0.10	0.16	0.27	0.07	0.02	0.05	0.32	0.25	0.05	0.02	
	180min		0.06	0.07	0.53	0.17	0.19	0.22	0.39	0.16	0.05	0.07	0.41	0.34	0.16	0.06	0.50	0.20	0.22	0.25	0.38	0.18	0.07	0.11	0.40	0.32	0.20	0.08	
Average			0.09	0.18	0.67	0.12	0.10	0.15	0.48	0.05	0.03	0.03	0.50	0.49	0.09	0.02	0.65	0.14	0.11	0.17	0.48	0.07	0.04	0.06	0.51	0.49	0.12	0.02	
Intensity	<1hr		15min	0.02	0.05	0.00	0.55	0.52	0.54	0.11	0.06	0.03	0.00	0.02	0.02	0.00	0.01	0.00	0.52	0.50	0.52	0.11	0.06	0.03	0.01	0.02	0.02	0.00	0.01
			60min	0.04	0.01	0.12	0.70	0.61	0.69	0.06	0.04	0.01	0.07	0.00	0.01	0.02	0.02	0.14	0.64	0.59	0.65	0.03	0.05	0.01	0.09	0.02	0.02	0.02	0.01
		180min	0.03	0.13	0.11	0.81	0.68	0.77	0.13	0.09	0.09	0.03	0.14	0.15	0.05	0.06	0.11	0.76	0.68	0.75	0.13	0.13	0.11	0.04	0.14	0.15	0.06	0.10	
	<3hr	15min	0.02	0.10	0.11	0.15	0.22	0.17	0.14	0.04	0.02	0.01	0.08	0.10	0.01	0.00	0.10	0.14	0.20	0.16	0.13	0.04	0.02	0.01	0.08	0.09	0.02	0.01	
		60min	0.01	0.06	0.01	0.31	0.45	0.37	0.10	0.02	0.02	0.03	0.07	0.07	0.02	0.05	0.01	0.28	0.43	0.34	0.09	0.03	0.02	0.06	0.06	0.05	0.04	0.05	
		180min	0.01	0.06	0.10	0.43	0.50	0.47	0.20	0.08	0.06	0.01	0.25	0.22	0.09	0.09	0.08	0.42	0.47	0.44	0.19	0.10	0.08	0.01	0.24	0.21	0.12	0.10	
	>3hr	15min	0.03	0.11	0.12	0.02	0.08	0.03	0.11	0.02	0.01	0.01	0.08	0.10	0.01	0.01	0.11	0.01	0.06	0.02	0.10	0.02	0.01	0.01	0.28	0.10	0.01	0.02	
		60min	0.02	0.06	0.08	0.07	0.17	0.11	0.09	0.02	0.00	0.03	0.06	0.04	0.02	0.04	0.05	0.06	0.16	0.10	0.08	0.02	0.00	0.05	0.05	0.03	0.04	0.04	
		180min	0.01	0.05	0.36	0.10	0.10	0.06	0.31	0.03	0.02	0.10	0.38	0.35	0.11	0.05	0.34	0.07	0.05	0.02	0.30	0.05	0.05	0.16	0.36	0.33	0.15	0.05	
	Average		0.02	0.07	0.11	0.35	0.37	0.36	0.14	0.04	0.03	0.03	0.12	0.12	0.03	0.04	0.10	0.32	0.35	0.33	0.13	0.05	0.04	0.05	0.12	0.11	0.05	0.04	
	Velocity X	<1hr	15min	0.04	0.02	0.09	0.01	0.01	0.00	0.06	0.14	0.17	0.02	0.06	0.05	0.01	0.02	0.08	0.01	0.01	0.00	0.08	0.13	0.18	0.02	0.14	0.07	0.02	0.02
			60min	0.03	0.03	0.12	0.03	0.02	0.02	0.04	0.31	0.37	0.06	0.10	0.03	0.01	0.03	0.11	0.04	0.02	0.03	0.04	0.33	0.52	0.09	0.15	0.04	0.00	0.03
180min			0.04	0.01	0.06	0.05	0.04	0.05	0.00	0.27	0.32	0.05	0.12	0.06	0.01	0.06	0.07	0.04	0.03	0.04	0.00	0.35	0.42	0.05	0.16	0.07	0.01	0.05	
<3hr		15min	0.03	0.06	0.10	0.02	0.01	0.01	0.06	0.03	0.07	0.01	0.05	0.04	0.01	0.02	0.08	0.02	0.00	0.02	0.05	0.03	0.06	0.01	0.15	0.03	0.02	0.03	
		60min	0.06	0.06	0.15	0.03	0.03	0.02	0.06	0.20	0.30	0.06	0.11	0.05	0.01	0.03	0.14	0.05	0.03	0.03	0.05	0.25	0.42	0.07	0.16	0.04	0.01	0.04	
		180min	0.04	0.01	0.10	0.03	0.02	0.02	0.02	0.27	0.26	0.04	0.13	0.07	0.00	0.06	0.10	0.02	0.02	0.02	0.02	0.29	0.38	0.05	0.18	0.07	0.00	0.05	
>3hr		15min	0.04	0.06	0.10	0.02	0.01	0.01	0.04	0.02	0.05	0.02	0.04	0.01	0.01	0.02	0.09	0.02	0.00	0.02	0.04	0.02	0.05	0.01	0.15	0.01	0.01	0.02	
		60min	0.04	0.04	0.05	0.04	0.03	0.04	0.04	0.07	0.16	0.05	0.00	0.04	0.00	0.02	0.04	0.05	0.03	0.04	0.05	0.08	0.23	0.07	0.15	0.05	0.02	0.02	
		180min	0.03	0.02	0.10	0.00	0.02	0.02	0.03	0.15	0.17	0.03	0.11	0.04	0.01	0.03	0.10	0.01	0.02	0.02	0.03	0.16	0.24	0.03	0.15	0.05	0.01	0.04	
Average		0.04	0.03	0.10	0.03	0.02	0.02	0.04	0.16	0.21	0.04	0.08	0.04	0.01	0.03	0.09	0.03	0.02	0.02	0.04	0.18	0.28	0.04	0.15	0.05	0.01	0.03		
Velocity Y		<1hr	15min	0.04	0.04	0.04	0.02	0.05	0.03	0.06	0.03	0.02	0.15	0.03	0.03	0.01	0.00	0.04	0.02	0.04	0.03	0.07	0.04	0.03	0.17	0.04	0.03	0.01	0.00
			60min	0.00	0.04	0.02	0.08	0.09	0.08	0.00	0.03	0.05	0.22	0.00	0.00	0.01	0.02	0.03	0.08	0.09	0.08	0.00	0.01	0.06	0.33	0.01	0.00	0.02	0.02
	180min		0.03	0.08	0.05	0.02	0.03	0.03	0.05	0.00	0.04	0.27	0.07	0.01	0.02	0.00	0.06	0.02	0.03	0.03	0.06	0.01	0.05	0.41	0.08	0.02	0.01	0.02	
	<3hr	15min	0.01	0.06	0.06	0.03	0.07	0.04	0.07	0.01	0.01	0.05	0.03	0.05	0.00	0.01	0.05	0.03	0.06	0.04	0.06	0.02	0.00	0.04	0.02	0.04	0.00	0.00	
		60min	0.01	0.06	0.02	0.04	0.10	0.06	0.03	0.01	0.06	0.18	0.02	0.05	0.01	0.01	0.00	0.04	0.11	0.06	0.03	0.00	0.07	0.26	0.01	0.04	0.01	0.01	
		180min	0.00	0.06	0.03	0.00	0.00	0.00	0.06	0.01	0.03	0.22	0.07	0.04	0.01	0.01	0.04	0.01	0.00	0.00	0.07	0.00	0.04	0.33	0.07	0.05	0.01	0.01	
	>3hr	15min	0.01	0.07	0.03	0.00	0.03	0.01	0.03	0.01	0.01	0.04	0.00	0.01	0.01	0.02	0.02	0.00	0.02	0.00	0.02	0.01	0.01	0.03	0.00	0.00	0.01	0.03	
		60min	0.03	0.02	0.02	0.01	0.03	0.01	0.07	0.00	0.04	0.09	0.09	0.08	0.01	0.01	0.04	0.01	0.03	0.00	0.09	0.01	0.07	0.16	0.10	0.10	0.01	0.00	
		180min	0.00	0.01	0.01	0.05	0.04	0.04	0.04	0.01	0.02	0.14	0.09	0.08	0.01	0.01	0.02	0.05	0.04	0.04	0.05	0.02	0.01	0.22	0.10	0.08	0.00	0.00	
	Average		0.01	0.05	0.03	0.03	0.05	0.03	0.05	0.01	0.03	0.15	0.04	0.04	0.01	0.01	0.03	0.03	0.05	0.03	0.05	0.01	0.04	0.22	0.05	0.04	0.01	0.01	
	Duration	Durations Lead Time	Cells	Lnow	A	lave	lmax	lstd1	lstd2	Vg	Vx	Vy	Jmax	Jmin	Jr	Φ	A ₃₀	lave ₃₀	lmax ₃₀	lstd1 ₃₀	lstd2 ₃₀	Vg ₃₀	Vx ₃₀	Vy ₃₀	Jmax ₃₀	Jmin ₃₀	Jr ₃₀	Φ ₃₀	
		Dur <1hr	0.06	0.16	0.31	0.02	0.04	0.00	0.22	0.03	0.03	0.00	0.19	0.24	0.00	0.03	0.30	0.02	0.03	0.01	0.21	0.03	0.03	0.01	0.19	0.25	0.01	0.04	
Dur <3hr		0.00	0.16	0.35	0.10	0.04	0.10	0.22	0.08	0.02	0.04	0.23	0.21	0.02	0.11	0.32	0.12	0.05	0.11	0.22	0.08	0.03	0.07	0.23	0.21	0.05	0.15		
Dur >3hr		0.07	0.02	0.43	0.20	0.18	0.21	0.21	0.15	0.04	0.04	0.25	0.16	0.14	0.01	0.40	0.22	0.20	0.23	0.20	0.18	0.07	0.07	0.23	0.14	0.18	0.01		
Average		0.04	0.11	0.36	0.11	0.09	0.10	0.22	0.09	0.03	0.03	0.22	0.20	0.05	0.05	0.34	0.12	0.09	0.12	0.21	0.10	0.04	0.05	0.22	0.20	0.08	0.07		

791

792

793



795

Appendix 11-3 The standard deviation of the Pearson Correlation Weights between predictors and target variables obtained from a cross-sampling of the events (leave one event at a time out). The boxplot for each target variable describes the spread of the standard deviation over all selected predictors.

796

12. References

797

Ayzel, G., Scheffer, T., & Heistermann, M. (2020). RainNet v1.0: A convolutional neural network for radar-based precipitation nowcasting. *Geoscientific Model Development*, 13(6). <https://doi.org/10.5194/gmd-13-2631-2020>

798

Bartels, H., Weigl, E., Reich, T., Lang, P., Wagner, A., Kohler, O., Gerlach, N., & MeteoSolutions GmbH. (2004). *Projekt RADOLAN - Routineverfahren zur Online-Aneicherung der Radarniederschlagsdaten mit Hilfe von automatischen Bodenniederschlagsstationen (Ombrometer)*.

800

801

Berenguer, M., Surcel, M., Zawadzki, I., Xue, M., & Kong, F. (2012). The diurnal cycle of precipitation from continental radar mosaics and numerical weather prediction models. Part II: Intercomparison among numerical models and with Nowcasting. *Monthly Weather Review*, 140(8), 2689–2705. <https://doi.org/10.1175/MWR-D-11-00181.1>

805

806

Berndt, C., Rabiei, E., & Haberlandt, U. (2014). Geostatistical merging of rain gauge and radar data for high temporal resolutions and various station density scenarios. *Journal of Hydrology*, 508, 88–101. <https://doi.org/10.1016/j.jhydrol.2013.10.028>

808

809

Berne, A., Delrieu, G., Creutin, J. D., & Obled, C. (2004). Temporal and spatial resolution of rainfall measurements required for urban hydrology. *Journal of Hydrology*, 299, 166–179. [https://doi.org/10.1016/S0022-1694\(04\)00363-4](https://doi.org/10.1016/S0022-1694(04)00363-4)

811

812

Bowler, N. E., Pierce, C. E., & Seed, A. W. (2006). STEPS: A probabilistic precipitation forecasting scheme which merges an extrapolation nowcast with downscaled NWP. *Quarterly Journal of the Royal Meteorological Society*, 132, 2127–2155. <https://doi.org/10.1256/qj.04.100>

814

815

Codo, M., & Rico-Ramirez, M. A. (2018). Ensemble radar-based rainfall forecasts for urban hydrological applications. *Geosciences (Switzerland)*, 8(8), 297. <https://doi.org/10.3390/geosciences8080297>

816

817

Dixon, M., & Wiener, G. (1993). TITAN: thunderstorm identification, tracking, analysis, and nowcasting - a radar-based methodology. *Journal of Atmospheric & Oceanic Technology*, 10(6), 785–797. [https://doi.org/10.1175/1520-0426\(1993\)010<0785:TTITAA>2.0.CO;2](https://doi.org/10.1175/1520-0426(1993)010<0785:TTITAA>2.0.CO;2)

819

820

Foresti, L., Reyniers, M., Seed, A., & Delobbe, L. (2016). Development and verification of a real-time stochastic

821 precipitation nowcasting system for urban hydrology in Belgium. *Hydrology and Earth System Sciences*, 20(1),
822 505-527. <https://doi.org/10.5194/hess-20-505-2016>

823 Galeati, G. (1990). A comparison of parametric and non-parametric methods for runoff forecasting. *Hydrological*
824 *Sciences Journal*, 35(1), 79–94. <https://doi.org/10.1080/02626669009492406>

825 Germann, U., & Zawadzki, I. (2004). Scale Dependence of the Predictability of Precipitation from Continental Radar
826 Images. Part II: Probability Forecasts. *Journal of Applied Meteorology*, 43(1), 74–89.
827 [https://doi.org/10.1175/1520-0450\(2004\)043<0074:SDOTPO>2.0.CO;2](https://doi.org/10.1175/1520-0450(2004)043<0074:SDOTPO>2.0.CO;2)

828 Germann, U., Zawadzki, I., & Turner, B. (2006). Predictability of precipitation from continental radar images. Part IV:
829 Limits to prediction. *Journal of the Atmospheric Sciences*, 63(8), 2092–2108. <https://doi.org/10.1175/JAS3735.1>

830 Gneiting, T., & Katzfuss, M. (2014). Probabilistic Forecasting. *Annual Review of Statistics and Its Application*, 1(1),
831 125–151. <https://doi.org/10.1146/annurev-statistics-062713-085831>

832 Goudenhoofdt, E., & Delobbe, L. (2013). Statistical characteristics of convective storms in Belgium derived from
833 volumetric weather radar observations. *Journal of Applied Meteorology and Climatology*.
834 <https://doi.org/10.1175/JAMC-D-12-079.1>

835 Grecu, M., & Krajewski, W. F. (2000). A large-sample investigation of statistical procedures for radar based short-term
836 quantitative precipitation forecasting. *Journal of Hydrology*, 239(1–4), 69–84. [https://doi.org/10.1016/S0022-](https://doi.org/10.1016/S0022-1694(00)00360-7)
837 [1694\(00\)00360-7](https://doi.org/10.1016/S0022-1694(00)00360-7)

838 Grünewald, U. (2009). *Zu Entstehung und Verlauf des extremen Niederschlags-Abfluss-Ereignisses am 26.07.2008 im*
839 *Stadtgebiet von Dortmund*.

840 Haberlandt, U. (2015). Stochastic simulation of daily lows for reservoir planning considering climate change .
841 *Hydrologie Und Wasserbewirtschaftung*, 59(5), 247–254. <https://doi.org/10.5675/HyWa-2015,5-5>

842 Han, L., Fu, S., Zhao, L., Zheng, Y., Wang, H., & Lin, Y. (2009). 3D convective storm identification, tracking, and
843 forecasting - An enhanced TITAN algorithm. *Journal of Atmospheric and Oceanic Technology*, 26(4), 719-732.
844 <https://doi.org/10.1175/2008JTECHA1084.1>

845 Hand, W. H. (1996). An object-oriented technique for nowcasting heavy showers and thunderstorms. *Meteorological*
846 *Applications*, 3, 31–41. <https://doi.org/10.1002/met.5060030104>

847 Hou, J., & Wang, P. (2017). Storm tracking via tree structure representation of radar data. *Journal of Atmospheric and*
848 *Oceanic Technology*, 34, 729–747. <https://doi.org/10.1175/JTECH-D-15-0119.1>

849 Imhoff, R. O., Brauer, C. C., Overeem, A., Weerts, A. H., & Uijlenhoet, R. (2020). Spatial and Temporal Evaluation of
850 Radar Rainfall Nowcasting Techniques on 1,533 Events. *Water Resources Research*, 56(8), 1–22.
851 <https://doi.org/10.1029/2019WR026723>

852 Jacobson, C. R. (2011). Identification and quantification of the hydrological impacts of imperviousness in urban
853 catchments: A review. *Journal of Environmental Management*, 92(6), 1438–1448.
854 <https://doi.org/10.1016/j.jenvman.2011.01.018>

855 Jasper-Tönnies, A., Hellmers, S., Einfalt, T., Strehz, A., & Fröhle, P. (2018). Ensembles of radar nowcasts and COSMO-
856 DE-EPS for urban flood management. *Water Science and Technology*, 2017(1), 27–35.
857 <https://doi.org/10.2166/wst.2018.079>

858 Jensen, D. G., Petersen, C., & Rasmussen, M. R. (2015). Assimilation of radar-based nowcast into a HIRLAM NWP
859 model. *Meteorological Applications*, 22(3), 485–494. <https://doi.org/10.1002/met.1479>

860 Johnson, J. T., Mackeen, P. L., Witt, A., Mitchell, E. D., Stumpf, G. J., Eilts, M. D., & Thomas, K. W. (1998). The storm
861 cell identification and tracking algorithm: An enhanced WSR-88D algorithm. *Weather and Forecasting*, 13(2),
862 263–276. [https://doi.org/10.1175/1520-0434\(1998\)013<0263:TSCIAT>2.0.CO;2](https://doi.org/10.1175/1520-0434(1998)013<0263:TSCIAT>2.0.CO;2)

863 Jung, S. H., & Lee, G. (2015). Radar-based cell tracking with fuzzy logic approach. *Meteorological Applications*, 22,
864 716–730. <https://doi.org/10.1002/met.1509>

865 Kato, A., & Maki, M. (2009). Localized heavy rainfall near Zoshigaya, Tokyo, Japan on 5 August 2008 observed by X-
866 band polarimetric radar - Preliminary analysis. *Scientific Online Letters on the Atmosphere*, 5(1), 89–92.
867 <https://doi.org/10.2151/sola.2009-023>

868 Kato, R., Shimizu, S., Shimose, K. I., Maesaka, T., Iwanami, K., & Nakagaki, H. (2017). Predictability of meso- γ -scale,
869 localized, extreme heavy rainfall during the warm season in Japan using high-resolution precipitation nowcasts.
870 *Quarterly Journal of the Royal Meteorological Society*, 153(704), 1406–1420. <https://doi.org/10.1002/qj.3013>

871 Kober, K., & Tafferner, A. (2009). Tracking and nowcasting of convective cells using remote sensing data from radar
872 and satellite. *Meteorologische Zeitschrift*, 18(1), 75–84. <https://doi.org/10.1127/0941-2948/2009/359>

873 Krämer, S. (2008). *Quantitative Radardatenaufbereitung für die Niederschlagsvorhersage und die*
874 *Siedlungsentwässerung*. Leibniz Universität Hannover.

875 Kyznarová, H., & Novák, P. (2009). CELLTRACK - Convective cell tracking algorithm and its use for deriving life
876 cycle characteristics. *Atmospheric Research*, 93(1–3), 317–327. <https://doi.org/10.1016/j.atmosres.2008.09.019>

877 L. Foresti, & Seed, A. (2015). On the spatial distribution of rainfall nowcasting errors due to orographic forcing.
878 *Meteorological Applications*, 22(1), 60–74.

879 Lall, U., & Sharma, A. (1996). A Nearest Neighbor Bootstrap For Resampling Hydrologic Time Series. *Water*
880 *Resources Research*, 32, 679–693. <https://doi.org/10.1029/95WR02966>

881 Lang, P. (2001). Cell tracking and warning indicators derived from operational radar products. *Proceedings of the 30th*
882 *International Conference on Radar Meteorology, Munich, Germany, i*, 245–247.
883 <http://link.springer.com/10.1007/s00376-014-0003-z>

884 Lin, C., Vasić, S., Kilambi, A., Turner, B., & Zawadzki, I. (2005). Precipitation forecast skill of numerical weather
885 prediction models and radar nowcasts. *Geophysical Research Letters*, 32, L14801.
886 <https://doi.org/10.1029/2005GL023451>

887 Lucas, B. ., & Kanade, T. (1981). Iterative Technique of Image Registration and Its Application to Stereo. *Proceedings*
888 *of the International Joint Conference on Neural Networks*, 674–679.

889 Moseley, C., Berg, P., & Haerter, J. O. (2013). Probing the precipitation life cycle by iterative rain cell tracking. *Journal*
890 *of Geophysical Research Atmospheres*, 118(24), 13,361-13,370. <https://doi.org/10.1002/2013JD020868>

891 Moseley, C., Henneberg, O., & Haerter, J. O. (2019). A Statistical Model for Isolated Convective Precipitation Events.
892 *Journal of Advances in Modeling Earth Systems*, 11(1). <https://doi.org/10.1029/2018MS001383>

893 Panziera, L., Germann, U., Gabella, M., & Mandapaka, P. V. (2011). NORA-Nowcasting of Orographic Rainfall by
894 means of analogues. *Quarterly Journal of the Royal Meteorological Society*, 137(661), 2106–2123.
895 <https://doi.org/10.1002/qj.878>

896 Pierce, C. E., Ebert, E., Seed, A. W., Sleigh, M., Collier, C. G., Fox, N. I., Donaldson, N., Wilson, J. W., Roberts, R., &
897 Mueller, C. K. (2004). The nowcasting of precipitation during Sydney 2000: An appraisal of the QPF algorithms.
898 *Weather and Forecasting*, 19(1), 7–21. [https://doi.org/10.1175/1520-0434\(2004\)019<0007:TNOPDS>2.0.CO;2](https://doi.org/10.1175/1520-0434(2004)019<0007:TNOPDS>2.0.CO;2)

899 Pierce, C., Seed, A., Ballard, S., Simonin, D., & Li, Z. (2012). Nowcasting. *Doppler Radar Observations - Weather*
900 *Radar, Wind Profiler, Ionospheric Radar, and Other Advanced Applications* (J. Bech and J. L. Chau (ed.); pp. 97–
901 142). <https://doi.org/10.5772/39054>

902 Rossi, P. J., Chandrasekar, V., Hasu, V., & Moisseev, D. (2015). Kalman filtering-based probabilistic nowcasting of
903 object-oriented tracked convective storms. *Journal of Atmospheric and Oceanic Technology*, 32(3), 461–477.
904 <https://doi.org/10.1175/JTECH-D-14-00184.1>

- 905 Ruzanski, E., Chandrasekar, V., & Wang, Y. (2011). The CASA nowcasting system. *Journal of Atmospheric and*
906 *Oceanic Technology*, 28(5), 640–655. <https://doi.org/10.1175/2011JTECHA1496.1>
- 907 Schellart, A., Liguori, S., Krämer, S., Saul, A., & Rico-Ramirez, M. A. (2014). Comparing quantitative precipitation
908 forecast methods for prediction of sewer flows in a small urban area. *Hydrological Sciences Journal*, 59(7), 1418–
909 1436. <https://doi.org/10.1080/02626667.2014.920505>
- 910 Sharma, A., & Mehrotra, R. (2014). An information theoretic alternative to model a natural system using observational
911 information alone. *Water Resources Research*, 50(1), 650–660.
912 <https://doi.org/https://doi.org/10.1002/2013WR013845>
- 913 Sharma, A., Mehrotra, R., Li, J., & Jha, S. (2016). A programming tool for nonparametric system prediction using
914 Partial Informational Correlation and Partial Weights. *Environmental Modelling & Software*, 83, 271–275.
915 <https://doi.org/https://doi.org/10.1016/j.envsoft.2016.05.021>
- 916 Shehu, B. (2020). *Improving the rainfall nowcasting for fine temporal and spatial scales suitable for urban hydrology*.
917 Leibniz Universität Hannover.
- 918 Shehu, B., & Haberlandt, U. (2021). Relevance of merging radar and rainfall gauge data for rainfall nowcasting in urban
919 hydrology. *Journal of Hydrology*, 594, 125931. <https://doi.org/https://doi.org/10.1016/j.jhydrol.2020.125931>
- 920 Surcel, M., Zawadzki, I., & Yau, M. K. (2015). A study on the scale dependence of the predictability of precipitation
921 patterns. *Journal of the Atmospheric Sciences*, 72(1), 216–235. <https://doi.org/10.1175/JAS-D-14-0071.1>
- 922 United, N. (2018). World Urbanization Prospects. In *Demographic Research*.
923 <file:///C:/Users/rocey/Downloads/WUP2018-Report.pdf>
- 924 Van Dijk, E., Van Der Meulen, J., Kluck, J., & Straatman, J. H. M. (2014). Comparing modelling techniques for
925 analysing urban pluvial flooding. *Water Science and Technology*, 69(2), 305. <https://doi.org/10.2166/wst.2013.699>
- 926 Wilson, J. W., Crook, N. A., Mueller, C. K., Sun, J., & Dixon, M. (1998). Nowcasting Thunderstorms: A Status Report.
927 *Bulletin of the American Meteorological Society*, 79(10), 2079–2099. [https://doi.org/10.1175/1520-0477\(1998\)079<2079:NTASR>2.0.CO;2](https://doi.org/10.1175/1520-0477(1998)079<2079:NTASR>2.0.CO;2)
- 928
- 929 Wilson, J. W., Feng, Y., Chen, M., & Roberts, R. D. (2010). Nowcasting challenges during the Beijing olympics:
930 Successes, failures, and implications for future nowcasting systems. *Weather and Forecasting*, 25(6), 1691–1714.
931 <https://doi.org/10.1175/2010WAF2222417.1>
- 932 Winterrath, T., Rosenow, W., & Weigl, E. (2012). On the DWD quantitative precipitation analysis and nowcasting
933 system for real-time application in German flood risk management. *IAHS-AISH Publication*, 351, 323–329.
- 934 Zahraei, A., Hsu, K. lin, Sorooshian, S., Gourley, J. J., Hong, Y., & Behrangi, A. (2013). Short-term quantitative
935 precipitation forecasting using an object-based approach. *Journal of Hydrology*, 483, 1–15.
936 <https://doi.org/10.1016/j.jhydrol.2012.09.052>
- 937 Zahraei, A., Hsu, K. lin, Sorooshian, S., Gourley, J. J., Lakshmanan, V., Hong, Y., & Bellerby, T. (2012). Quantitative
938 Precipitation Nowcasting: A Lagrangian Pixel-Based Approach. *Atmospheric Research*, 118, 418–434.
939 <https://doi.org/10.1016/j.atmosres.2012.07.001>
- 940 Zawadzki, I. I. (1973). Statistical Properties of Precipitation Patterns. *Journal of Applied Meteorology*, 12(3), 459–472.
941 [https://doi.org/10.1175/1520-0450\(1973\)012<0459:sppop>2.0.co;2](https://doi.org/10.1175/1520-0450(1973)012<0459:sppop>2.0.co;2)
- 942 Zou, X., Dai, Q., Wu, K., Yang, Q., & Zhang, S. (2020). An empirical ensemble rainfall nowcasting model using multi-
943 scaled analogues. *Natural Hazards*, 103(1), 165–188. <https://doi.org/10.1007/s11069-020-03964-3>